Pharmacological Research 151 (2020) 104567

Contents lists available at ScienceDirect

Pharmacological Research

journal homepage: www.elsevier.com/locate/yphrs

Invited Review

The role of fibroblast growth factor receptor (FGFR) protein-tyrosine kinase inhibitors in the treatment of cancers including those of the urinary bladder

Robert Roskoski Jr.

Blue Ridge Institute for Medical Research, 3754 Brevard Road, Suite 116, Box 19, Horse Shoe, NC, 28742-8814, United States

ARTICLE INFO

Chemical compounds studied in this article:
AZD4547 (PubMED CID: 51039095)
Dovitinib (PubMED CID: 135398510)
Erdafitinib (PubMED CID: 67462786)
Infigratinib (PubMED CID: 53235510)
Lucitanib (PubMED CID: 25031915)
Nintedanib (PubMED CID: 135423438)
Pazopanib (PubMED CID: 10113978)
Pemigatinib (PubMED CID: 86705695)
Ponatinib (PubMED CID: 24826799)
Rogaratinib (PubMED CID: 71611869)

Keywords:
Catalytic spine
K/E/D/D
Protein kinase inhibitor classification
Protein kinase structure
Regulatory spine
Targeted cancer therapy

ABSTRACT

The human fibroblast growth factor family consists of 22 factors and five transmembrane receptors. Of the 22 factors, eighteen are secreted while four of them function exclusively within the cell. Four of the fibroblast growth factor receptors (FGFRs) possess intracellular protein-tyrosine kinase activity while the fifth (FGFRL1) has a short 105-residue intracellular non-enzymatic component. The FGFR protein kinase domain consists of a bi-lobed structure that is similar to that of all other protein kinases. *FGFR* gene alterations occur in a wide variety of cancers including those of the urinary bladder, breast, ovary, prostate, endometrium, lung, and stomach. The majority (66 %) of *FGFR* gene alterations involve gene amplifications, followed by mutations (26 %), and rearrangements that produce fusion proteins (8 %). Erdafitinib was the first orally effective FGFR antagonist approved by the FDA (2019) for the treatment of advanced cancer, that of the urinary bladder. FGF23 suppresses phosphate reabsorption in the proximal tubules of the kidney; FGF23 blockade allows phosphate reabsorption to occur and leads to elevated serum phosphate levels. Erdafitinib and several other, but not all, FGFR antagonists produce hyperphosphatemia. Erdafitinib binds to an inactive DGF-D_{in} conformation of FGFR1 and is classified as a type I½ inhibitor. Similarly, dovitinib, AZD4547, CH5183284, infigratinib, lenvatinib, LY2874455, and lucitanib are type I½ inhibitors. The inactive conformations contain an autoinhibitory brake that is made up of three main residues: an asparagine (N) within the αC-β4 back loop, a glutamate (E) corresponding to the second hinge residue, and a lysine (K) in the β8-strand (the NEK triad). PDGFRα/β, Kit, CSF1R, VEGFR1/2/3, Flt3, Tek, and Tie protein kinases are also regulated by a similar autoinhibitory brake mechanism. Ponatinib binds to FGFR4 in a DFG-D_{out} conformation and is classified as a type II inhibitor. Futibatinib, roblitinib, H3B-6527, fisogatinib, and PRN1371 bind covalently to their FGFR target and are classified as type VI inhibitors. Nintedanib, pazopanib, pemigatinib, rogaratinib, fisogatinib, and PRN1371 are FGFR inhibitors lacking drug-enzyme crystal structures. All of the aforementioned FGFR antagonists are orally effective. The development of FGFR inhibitors has lagged behind those of other receptor protein-tyrosine kinases. However, the FDA approval of erdafitinib for the treatment of urinary bladder cancers may stimulate additional work targeting the many other FGFR-driven neoplasms.

1. Fibroblast growth factors and their receptors

1.1. Properties of the fibroblast growth factors

The human fibroblast growth factor (FGF) family consists of 22 members [1]. Although these are labeled FGF1–23, factors 15 and 19 represent the same molecule that is called FGF15/19 in this paper; thus, the total number of FGFs is 22. All of the growth factors, with the exception of FGF11/12/13/14, are glycoproteins that are secreted from the cell of origin and they interact with the transmembrane fibroblast growth factor receptors (FGFRs). FGF11/12/13/14 do not interact with the transmembrane FGFRs; of the 22 FGFs, a total of 18 of these function as receptor ligands. The intracellular growth factors (FGF11/12/13/14) serve as cofactors for voltage-gated sodium channels. The growth factors range in size from 155 residues (FGF1) to 288 residues (FGF2) (Table 1). These factors share a core homology domain that consists of about 120 amino acid residues that assume a globular β-trefoil structure that consists of 12 β-strands arranged into three similar sets of four-stranded β-sheets [2]. This core domain is flanked by divergent amino-terminal and carboxyterminal sequences that account in

Abbreviations: AS, activation segment; CS or C-spine, catalytic spine; CL, catalytic loop; EGFR, epidermal growth factor receptor; GK, gatekeeper; GRL, glycine-rich loop; KID, kinase insert domain; NSCLC, non-small cell lung cancer; PDGFR, platelet-derived growth factor receptor; PI3K, phosphoinositide 3-kinase; pY or pTyr, phosphotyrosine; RS or R-spine, regulatory spine; Sh2, shell residue 2; VEGFR, vascular endothelial growth factor receptor

E-mail address: rrj@brimr.org.

https://doi.org/10.1016/j.phrs.2019.104567
Received 20 November 2019; Accepted 20 November 2019
Available online 23 November 2019

Table 1
Fibroblast growth factor and fibroblast growth factor receptor properties and interactions.[a]

Name	Symbol	Residues	MW (kDa)	UniprotKB ID	Comments
Fibroblast growth factors					
Fibroblast growth factor 1	FGF1	155	17.5	P05230	Acidic FGF; interacts with FGFR1/2/3/4
Fibroblast growth factor 2	FGF2	288	30.7	P09038	Basic FGF; interacts with FGFR1/2/3/4
Fibroblast growth factor 3	FGF3	239	26.9	P11487	Interacts with FGFR1/2
Fibroblast growth factor 4	FGF4	239	22.0	P08620	Interacts with FGFR1/2/3/4
Fibroblast growth factor 5	FGF5	268	29.5	P12034	Interacts with FGFR1/2
Fibroblast growth factor 6	FGF6	208	22.9	P10767	Interacts with FGFR1/2/4
Fibroblast growth factor 7	FGF7	194	22.5	P21781	Interacts with FGFR2/4
Fibroblast growth factor 8	FGF8	233	26.5	P55075	Interacts with FGFR1/2/3/4; androgen-induced growth factor
Fibroblast growth factor 9	FGF9	208	23.4	P31371	Interacts with FGFR2/3/4; glia-activating factor
Fibroblast growth factor 10	FGF10	208	23.4	O15520	Interacts with FGFR1/2
Fibroblast growth factor 11	FGF11	225	25.0	Q92914	FGF homologous factor 3; nervous system function
Fibroblast growth factor 12	FGF12	243	27.4	P61328	FGF homologous factor 1; nervous system function, cytosolic and nuclear localization
Fibroblast growth factor 13	FGF13	245	27.6	Q92913	FGF homologous factor 2; nervous system function, nuclear localization
Fibroblast growth factor 14	FGF14	247	27.7	Q92915	FGF homologous factor 4; nervous system function, nuclear localization
Fibroblast growth factor 15	FGF15/19	216	24.0	O95750	Interacts with FGFR1/2/3/4 and β-Klotho; 15/19 are the same
Fibroblast growth factor 16	FGF16	207	23.8	O43320	Interacts with FGFR2/3/4; S111 is phosphorylated
Fibroblast growth factor 17	FGF17	216	24.9	O60258	Interacts with FGFR1/2/3/4
Fibroblast growth factor 18	FGF18	207	24.0	O76093	Interacts with FGFR2/3/4
Fibroblast growth factor 19	FGF15/19	216	24.0	O95750	Interacts with FGFR1/2/3/4; 15/19 are the same
Fibroblast growth factor 20	FGF20	211	23.5	Q9NP95	Interacts with FGFR1/2/3/4
Fibroblast growth factor 21	FGF21	209	22.3	Q9NSA1	Interacts with FGFR1/2/3/4 and β-Klotho
Fibroblast growth factor 22	FGF22	170	19.7	Q9HCT0	Interacts with FGFR1/2
Fibroblast growth factor 23	FGF23	251	28.0	Q9 GZV9	Interacts with FGFR1/2/3/4 and α-Klotho; hypophosphatemia-inducing factor
Fibroblast growth factor receptors					
Fibroblast growth factor receptor 1	FGFR1/Flt2	822	91.9	P11362-1 & P11362-19	FGF1–6/8/10/17/19–23; isoforms IIIb & IIIc;
Fibroblast growth factor receptor 2	FGFR2	821/822	92.0/92.0	P21802-1 & P21802-3	FGF1–10/16–23; isoforms IIIb & IIIc
Fibroblast growth factor receptor 3	FGFR3	806/808	87.7/88.2	P22607-1 & P22607-2	FGF1/2/4/8/9/16–21/23; isoforms IIIb & IIIc
Fibroblast growth factor receptor 4	FGFR4	802	88.0	P22455	FGF1/2/4/6–9/16–21/23; one isoform
Fibroblast growth factor receptor like	FGFRL1	504	54.5	Q8 N441	No protein kinase domain

[a] Data from UniprotKB and Ref. [1].

part for the selectivity and specificity of the growth factors.

The FGFs are divided into six subfamilies. The first subfamily (FGF1) consists of FGF1 and FGF2 [3]. Although these factors lack a traditional signal peptide, they are readily exported from cells by coursing through the plasma membrane. FGF1/2 bind to and activate their cognate FGFRs (Table 1). These factors have the unusual property of being translocated back into the cell through the plasma membrane and traveling through the cytosol into the nucleus. Postulated nuclear functions include regulation of the cell cycle, cell differentiation, cell survival, and apoptosis. The second subfamily (FGF4) consists of FGF4, FGF5, and FGF6. These factors are secreted from the cell with a cleavable N-terminal signal peptide. These secreted factors interact with and activate their cognate FGFRs.

The third subfamily (FGF7) consists of FGF3, FGF7, FGF10, and FGF22 [3]. These factors possess a signal peptide and are secreted from cells. FGF3/10/22 interact with FGFR1/2 while FGF7 interacts with FGFR2/4. The fourth subfamily (FGF8) consists of FGF8, FGF17, FGF18. These factors are secreted from the cell by the classical signal peptide pathway and FGF8/17 interacts with FGFR1/2/3/4 and FGF18 interacts with FGFR2/3/4. The fourth subfamily (FGF9) consists of FGF9, FGF16, and FGF20. These factors are secreted from cells and interact with and activate their corresponding receptors (Table 1). These proteins function as homodimers. The fifth subfamily (FGF15/19) consists of FGF15/19, FGF21, and FGF23. These growth factors are secreted from cells by the classical signal peptide process and they interact with FGFR1/2/3/4. All of the previous FGFs function close to the cell that secreted them in an autocrine or paracrine fashion owing to their high affinity for extracellular heparan sulfate glycosaminoglycan chains of heparan sulphate proteoglycans. Moreover, heparan sulfate participates in the FGF-FGFR interaction through the formation of ternary complexes made up of the three components (FGF-FGFR-heparan). The paracrine FGFs include the FGF1, FGF4, FGF7, and the FGF8 subfamilies while the endocrine FGFs consists of the FGF15/19 subfamily.

In contrast to the subfamilies 1–4, the FGF15/19 family is carried by the circulation to their target cells and receptors and they function as endocrine factors; these factors possess low affinity for heparan sulfate, which allows them to diffuse from the site of origin into the circulation and travel to their targets [3]. These endocrine factors form a ternary complex with their receptors and their α-Klotho or β-Klotho coreceptors (FGF-FGFR-Klotho). α-Klotho and β-Klotho are single pass transmembrane proteins consisting of about one thousand amino acid residues with short cytoplasmic domains: α-Klotho with 10 intracellular residues and β-Klotho with 27 intracellular residues. FGF15/19 and FGF21 signaling involves β-Klotho. FGF15/19 can activate FGFR1-IIIc, FGFR2-IIIc, FGFR3-IIIc, and FGFR4. FGF21 activates FGFR1-IIIc and FGFR3-IIIc (where the IIIb and IIIc isoforms result from alternative spicing as described in the next section). FGF23 involves α-Klotho and FGFR1-IIIc, FGFR3-IIIc, and FGFR4. The discrepancies in the binding of the FGF15/19 family to their receptors described here and in Table 1 are related to variations in the findings reported by different groups [1,3].

The sixth FGF subfamily (FGF11) consists of FGF11, FGF12, FGF13, and FGF14 [3]. These factors are not secreted and occur within the cytosol and nucleus [3]. This subfamily interacts with the cytosolic carboxyterminal tail of voltage-gated sodium channels. These polypeptides may regulate the localization of sodium channels at the axon terminus during development and the ion-gating properties of the channels in mature neurons. It is possible that these factors are involved in ion-gating properties of excitable cells including cardiomyocytes.

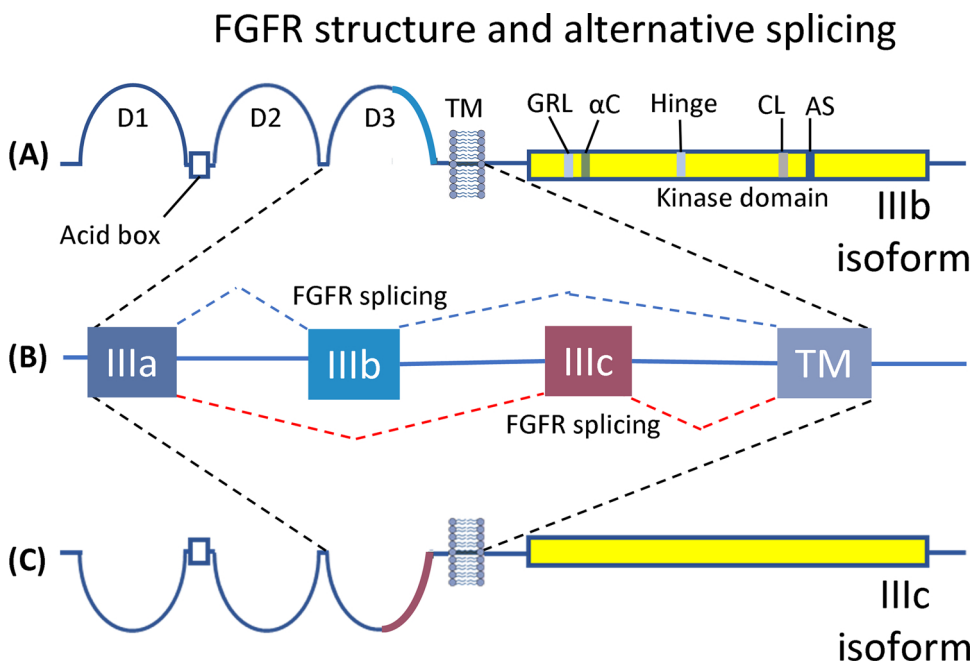

Fig. 1. FGFR overall structure and isoforms produced by alternative pre-mRNA splicing. D1, immunoglobulin-like domain 1; TM, transmembrane segment; GRL, glycine-rich loop; CL, catalytic loop; AS, activation segment.

1.2. Properties of the fibroblast growth factor receptors

1.2.1. Ligand activation of the FGFRs

The FGFRs consist of an extracellular segment containing three immunoglobulin-like domains (D1/2/3), a single-pass transmembrane segment, and an intracellular protein-tyrosine kinase domain (Fig. 1). An acid box consisting of a short stretch of aspartates and glutamates occurs between D1 and D2. FGFs bind to the region of the ectodomain encompassing D2, D3, and the D2-D3 linker (Fig. 2). Ligand-binding specificity of FGFR1/2/3 is regulated in part by alternative splicing in the D3 domain of these receptors (Fig. 1). The N-terminal portion of D3 is encoded by exon IIIa (also known as exon 7) and the C-terminal portion of D3 is encoded by one of two mutually exclusive exons (exon IIIb or exon IIIc, also known as exon 8 or exon 9) where III refers to D3. Structural studies demonstrate that alternative splicing changes the sequence of key ligand-pocket residues or ligand-binding residues to confer FGF binding specificity. This alternative splicing is largely cell and tissue specific [2]. FGFR4 mRNA does not undergo alternative splicing of the encoded D3 domains.

The binding of the FGFs to their receptors induces receptor

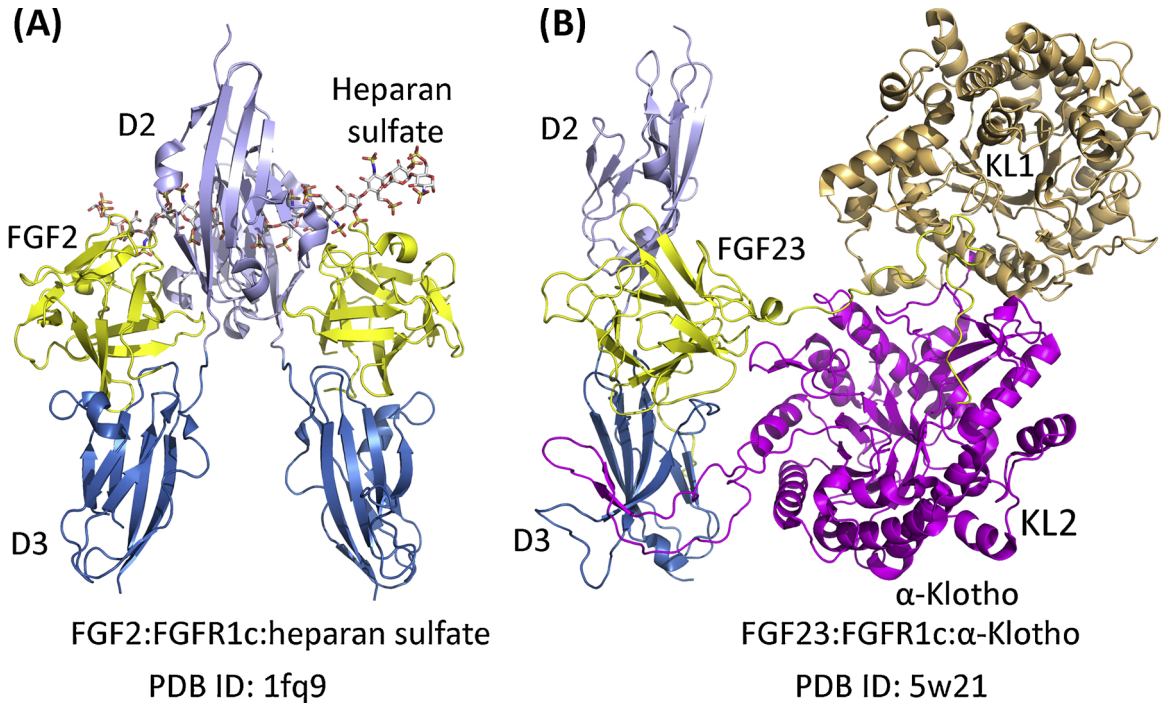

Fig. 2. Fibroblast growth factors bind to the D2-D3 domains of their receptors. (A) FGF-FGFR-heparan-sulfate complexes. (B) FGF-FGFR-αKlotho complexes. KL1 and KL2 are the major components of Klotho.

dimerization, transphosphorylation, and activation of the protein kinase domain [4]. Six tyrosine residues of FGFR1 are sequentially phosphorylated to produce the fully activated enzyme [5]. In the first phase following ligand binding, Y653 within the activation segment is phosphorylated resulting in a 50-100–fold increase in activity. In the second phase, Y583 in the kinase insert domain (KID), Y463 in the juxtamembrane segment, Y766 at the end of the protein kinase domain, and Y585 in the αD-αE loop are phosphorylated. In the third phase, Y654 within the activation segment is phosphorylated resulting in a further 10-fold activation (overall 500-1000–fold activation). The equivalent tyrosine residues of FGFR2 are phosphorylated; whether the order of phosphorylation and activation parallels that described for FGFR1 is unclear. FGFR3 contains only four phosphotyrosines including two adjacent residues within the activation segment and FGFR4 contains only three phosphotyrosines including two adjacent residues within the activation segment. Clearly the phosphorylation pattern of FGFR3/4 must differ from that of FGFR1.

Downstream signaling by the FGFRs resembles that of most other receptor protein-tyrosine kinases including its close relatives consisting of Kit, PDGFRα/β, VEGFR1/2/3, EGFR/ErbB1/2/3/4, and RET. All four FGFRs result in the activation of the Ras-Map kinase signaling module that participates in cell division and the PI3K/Akt module that mediates cell survival [2,6]. They also lead to the activation of phospholipase C and the generation of inositol-trisphosphate and diacylglycerol, which promote cell migration. The four enzymes also promote the activation of the STAT (signal transducer and activator of transcription) pathway leading to the transcription of numerous genes. The activation of downstream pathways appears to be qualitatively similar for FGFR1 and FGFR2 and differs somewhat from that of FGFR3 and FGFR4. Dissimilarities among the four receptors in downstream signaling can be ascribed to differences in the affinity and specificity for intracellular adaptor proteins, differential subcellular trafficking after receptor activation, and differential rates of receptor endocytosis.

The paracrine family of FGFs binds to their cognate receptors in a process that is aided by the extracellular heparan sulfate glycosaminoglycan chains of heparan sulphate proteoglycans [2,4]. Heparan sulfate consists of a long linear chain of repeating sulfated disaccharides including glucuronic acid linked to *N*-acetylglucosamine. These chains are covalently bound to various core proteins such as agrin, glypican, perlecan, and syndecan. Heparan sulfate interacts with FGFs and FGFRs to form a symmetric 2:2:2 FGF-heparan-FGFR complex. FGFR dimerization leads to the transphosphorylation and activation of the receptor. The heparan sulfate links the FGF to the D2 extracellular domain (Fig. 2A).

The endocrine family of FGFs binds to their cognate receptors in a process that is aided by a Klotho co-receptor [6,7]. Chen et al. determined the X-ray crystal structure of FGF23, FGFR1, and the extracellular domain of α-Klotho (Fig. 2B) [7]. They reported that α-Klotho serves as a non-enzymatic scaffold that tethers FGF23 and FGFR1-IIIc together. KL1 (^{34}E–F^{506}) and KL2 (^{515} L–S^{950}) are two domains within α-Klotho that are connected by a ^{507}P–P^{514} linker (not shown) and the two domains interact with FGF23; most of the interaction involves KL2 via hydrophobic contacts as well as hydrogen bonding. α-Klotho binds within a large hydrophobic groove and a smaller hydrophobic groove both within FGFR1-IIIc. These hydrophobic pockets in FGFR1 differ between the IIIb and IIIc isoforms accounting in part for the binding selectivity of α-Klotho for this subset of FGFRs. These investigators found that heparan sulfate was a required ancillary cofactor that was needed to promote the formation functional 2:2:2:2 FGF23:FGFR1-IIIc:Klotho:heparan sulfated complexes. This was a surprising finding because both FGF23 and FGFR1-IIIc have limited binding affinity for heparan sulfate.

1.2.2. Structures of the FGFR protein-tyrosine kinases and the K/E/D/D motif

Receptor protein-tyrosine kinases consist of 58 distinct members that have been divided into 20 subfamilies [4,8]. As previously described, the FGFR subfamily consists of four protein kinases (FGFR1/2/3/4) plus a non-protein kinase (FGFRL1). Each of the protein-tyrosine kinases catalyze the following reaction:

$$MgATP^{-1} + \text{protein–tyrosine-O: H} \rightarrow \text{protein–-tyrosine-O: } PO_3^{2-} + MgADP + H^+$$

Note that the phosphorylium group (PO_3^{2-}) and not the phosphate group (OPO_3^{3-}) is transferred in this reaction. The FGFRs are closely related to PDGFRα/β, Kit, CSF1R, and VEGFR1/2/3. The protein kinase domain of each of these receptors contains an insert of several amino acids; the kinase insert domain (KID) consists of nearly 100 residues in the PDGFR family, about 60 residues in Kit, CSF1R and the VEGFR family, and about 15 amino acid residues in the FGFR family [9]. Phosphorylation of two tyrosine residues within the KIDs of FGFR1 and FGFR2 has been reported, but no tyrosine phosphorylation of the KIDs of FGFR3 or FGFR4 has been found.

The secondary and tertiary structures of all protein kinases are similar as first described by Knighten et al. for protein kinase A [10,11]. Protein kinases contain a small N-terminal lobe and a large C-terminal lobe (Fig. 3A). The small N-terminal lobe contains five β-strands and the large C-terminal lobe is mostly helical; it contains eight helices (αD–αI and αEF1/2) along with four short β-strands (β6–β9). The small lobe contains an important regulatory αC-helix. This lobe also contains a glycine-rich loop (GRL) with a six amino acid-signature sequence (GxGxΦG) where Φ represents a hydrophobic residue; in the case of FGFRs, Φ is phenylalanine (Table 2). The glycine-rich loop connects the β1 and β2-strands (Fig. 3E) and sits above the adenine binding site (not shown). The β3-strand of protein kinases contains an AxK signature sequence, which is AVK in the FGFR family. In the active enzyme conformation (and many inactive conformations), this invariant lysine forms a salt bridge with an invariant glutamate within the αC-helix; this corresponds to β3-K514 and αC-E531 in FGFR1 (Fig. 3C). The salt-bridge conformation is described as the αC_{in} structure. Enzyme conformations lacking this salt bridge are described as αC_{out} or $\alpha C_{dilated}$ structures; see Refs. [12,13] for details. The β3-lysine (*K*) and the αC-glutamate (*E*) make up the *K* and *E* of the *K/E/*D/D signature.

The hinge region and linker (which we combine and call the hinge) are made up of about seven amino acid residues that connect the small and large lobes (Fig. 3C, Table 2). The gatekeeper residue occurs immediately before the hinge residues in the β5-strand. The term gatekeeper refers to the role that such residues play in regulating access to a hydrophobic pocket next to the adenine binding site [14,15] that is occupied by fragments of numerous small molecule protein kinase inhibitors. Small residues such as alanine, glycine, serine, cysteine, threonine, and valine enable antagonists to extend into the hydrophobic pocket while medium-sized residues including leucine, isoleucine, glutamine, and methionine are more obstructive [16]. Large residues such as tyrosine and phenylalanine are the most obstructive and preclude extension of antagonists or drugs into the hydrophobic back pocket. The small kinase insert domain of the FGFRs occupies the αD–αE loop (Fig. 3A). The KID of FGFR1/2 contains two tyrosine residues that are phosphorylated and these may participate in the mitogenic response via the phospholipase Cγ and Ras signaling modules [9]. The KID of FGFR3 contains a single tyrosine residue, but it has not been shown to be phosphorylated. The KID of FGFR4 lacks any tyrosine residues, but it contains a serine (S573) that is phosphorylated, presumably by a protein-serine/threonine kinase. Whatever regulatory role that phosphorylation of this serine plays, if any, is unclear.

An evolutionarily conserved protein kinase catalytic loop, which consists of $HRD(x)_4N$, occurs after the αE helix and before the β7-strand (Fig. 3A). The catalytic loop aspartate of all protein kinases including the FGFR family serves as a base that abstracts a proton from the tyrosyl −OH group. This aspartate represents the first *D* of the K/E/*D*/D motif. Mechanistic studies by Zhou and Adams suggested that this protein

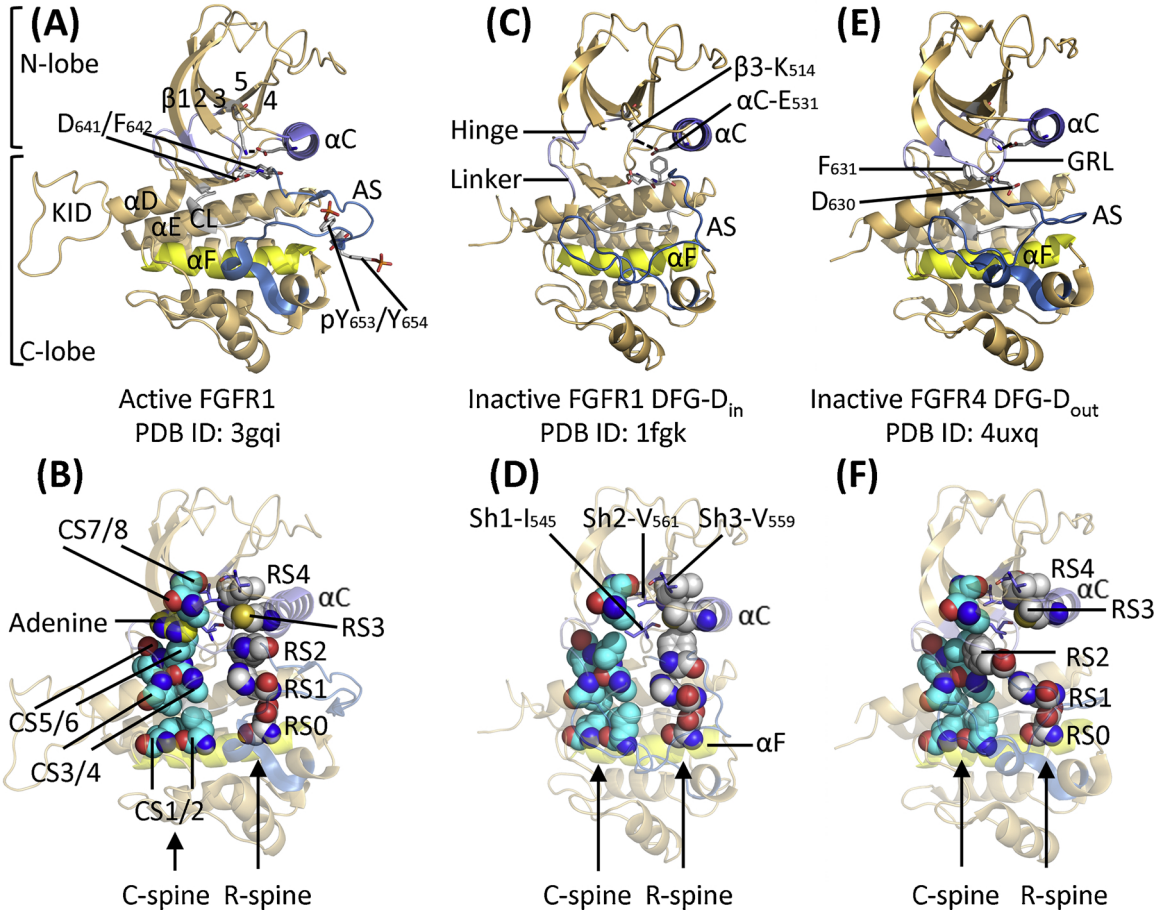

Fig. 3. Structures of active (A) and inactive (C, E) FGFRs along with the depiction of their corresponding catalytic and regulatory spines and shell residues (B, D, and F). The dashed lines in this figure and in figures 4–6, 9, and 10 represent hydrogen bonds. AS, activation segment; CL, catalytic loop; CS1, catalytic spine residue-1; KID, kinase insert domain; RS2, regulatory spine residue-2; Sh3, shell residue-3.

Table 2
Important residues in human FGFR receptors.

	FGFR1	FGFR2	FGFR3	FGFR4
Number of residues	822	821	806	802
Signal peptide	1–21	1–21	1–22	1–21
Extracellular segment	22–376	22–377	23–375	22–369
Ig-like domain 1 (D1)	25–119	25–125	24–126	22–118
Acid box	126–138	132–142	132–143	126–129
Ig-like domain 2 (D2)	158–246	154–247	151–244	152–240
Ig-like domain 3 (D3)	255–357	256–358	253–355	249–349
Transmembrane segment	377–397	378–398	376–396	370–390
Intracellular segment	398–822	399–821	397–806	391–802
Protein kinase domain	478–767	481–770	472–761	467–755
Glycine-rich loop, GEGCFG	485–490	488–493	479–484	474–480
The K of *K*/E/D/D, or the β3-lysine	514	517	508	503
β3-AVK	512–514	515–517	506–508	501–503
Molecular brake triad	N546, E562, K638	N549, E565, K641	N540, E556, K632	N535, E551, K627
αC-E residue	531	534	525	520
Hinge residues	562–568	565–571	556–562	551–557
	EYASKGN	EYASKGN	EYAAKGN	ECAAKGN
Gatekeeper residue	V561	V564	V555	V550
Kinase insert domain (KID)	^{580}GLE*Y*SYN PSHNPEEQ^{594}	^{583}GME*Y*SYDI NRVPEEQ^{597}	^{574}GLDYSFDT CKPPEEQ^{588}	^{569}GPDL*S*PDGP RSSEGP^{584}
Catalytic HRD residue, the first D of K/E/*D*/D	623	626	617	612
Catalytic loop N (HRD(x)$_4$*N*	628	631	622	617
Activation segment DFG, the second D of K/E/D/*D*	641	644	635	630
Activation segment tyrosine phosphorylation sites	Y653/4	Y656/7	Y647/8	Y642/3
End of the activation segment, APE	668–670	671–673	662–664	657–659
Molecular weight (kDa)	91.9	92.0	87.7	87.9
UniProtKB ID	P11362	P21802	P22607	P22455

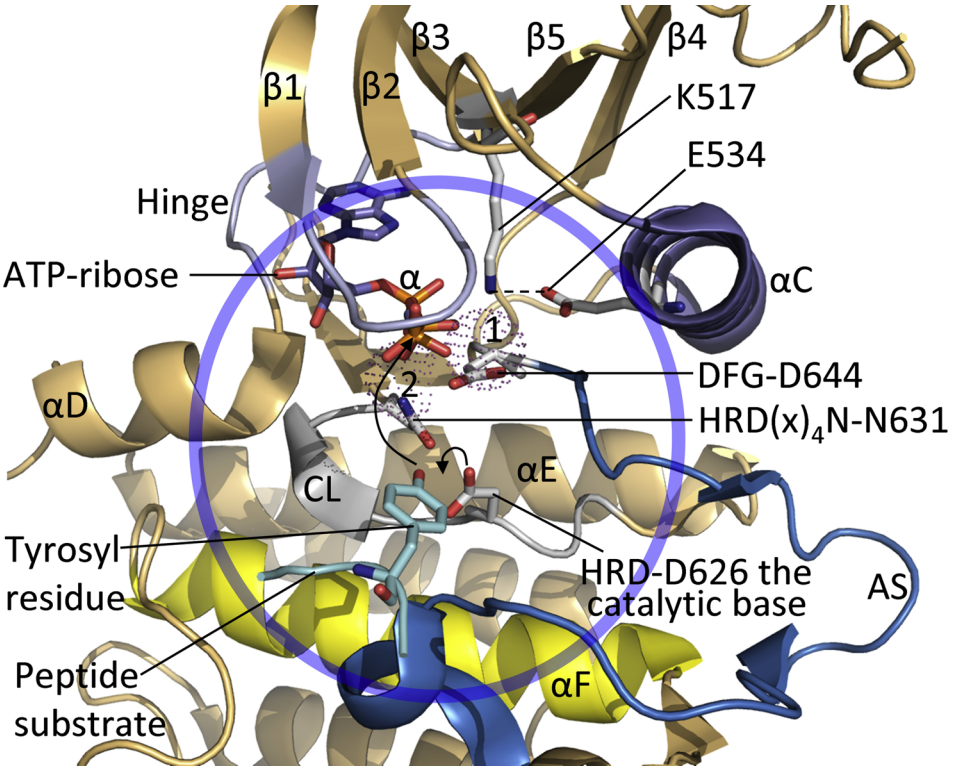

Fig. 4. Inferred mechanism of the FGFR2-catalyzed protein kinase reaction. HRD-D626 abstracts a proton from the peptidyl tyrosyl substrate allowing for its nucleophilic attack onto the γ-phosphorus atom of ATP. 1 and 2 label the two Mg^{2+} ions shown as dots. The chemistry occurs within the circle. AS, activation segment; CL, catalytic loop; The figure was prepared from PDB ID: 2pvf.

kinase catalytic aspartate promotes the in-line nucleophilic attack of the hydroxyl group of the protein substrate [17]. The activation segment of protein kinases represents an important structural and regulatory protein kinase component. This segment begins with a DGF sequence and usually, but not always, ends with an APE sequence. The *D* of *D*FG represents the second *D* of the K/E/D/*D* motif. Two magnesium ions (Mg^{2+}) are involved in the transphosphorylation reaction of nearly all protein kinases [18,19]. The DFG-*D* binds Mg^{2+}(1) and the *N* of HRD $(x)_4N$ binds Mg^{2+}(2). The inferred mechanism of the FGFR2 catalyzed reaction is depicted in Fig. 4.

The activation segment of protein kinases exhibits an active conformation with the DFG-D-Mg^{2+}(1) pointing inward toward the active site (DFG-D_{in}) and with an open conformation that extends rightward in the classical protein kinase view (Fig. 1A). One common dormant activation segment conformation also has DFG-D_{in}, but with a closed activation segment conformation that does not extend as far rightward (Fig. 1C). Still a second inactive conformation has the DFG-D directed away from the active site (DFG-D_{out}) as illustrated in Fig. 3E. In the case of FGFR1, the phosphate of the second phosphotyrosine (pY654) forms salt bridges with the guanidinium group of R646 – which is eight residues upstream in the activation segment – and with the hydroxyl group of T657, which is three residues downstream within the activation segment (Fig. 5). The carbonyl group of pY654 forms a hydrogen bond with the N—H group of Y677, which is proximal to the αF-helix. pY653 is exposed to the solvent and does not play a role in stabilizing the activation segment in its active conformation. Y653, Y654, T657, and R646 of the dormant enzyme are displaced relative to the corresponding residues of the active enzyme. In contrast, Y677 of the dormant enzyme and Y677 of the active enzyme, which are outside of the activation segments, are nearly superimposable.

Chen et al. first described the regulation of FGFR2 by an autoinhibitory molecular brake [20]. FGFR1/3/4, PDGFRα/β, VEGFR1/2/3, Kit, CSF1R, Flt3, Tek, and Tie protein kinases are also regulated by a similar autoinhibitory mechanism. This process involves three main residues: a lysine (K) in the β8-strand, a glutamate (E) corresponding to the second hinge residue, and an asparagine (N) within the αC-β4 back

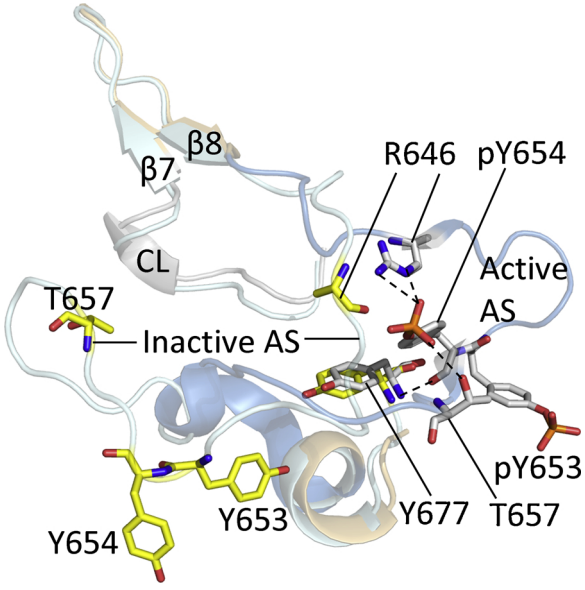

Fig. 5. Superposition of active (blue, PDB ID: 3gqi) and dormant activation segments (cyan, PDB ID: 1fgk) of FGFR1. The activation segment of the functional enzyme is extended toward the right in an open conformation and that of the dormant enzyme is in a closed conformation. The gray residues are in the active enzyme and the yellow residues are in the dormant enzyme. AS, activation segment; CL, catalytic loop.

loop, together making a KEN triad. The hydrogen bonding pattern for these three residues in FGFR1 is illustrated in Fig. 6A. A hydrogen bond forms between the side chain of K638 and the carboxylate side chain of E562 and another occurs between the carboxylate side chain of E562 and the backbone N—H group of N546. The N—H group of E562 hydrogen bonds with the carbonyl group of N546. Moreover, two polar bonds link the carboxylate side chain of E562 with the amide side chain of N546. The carboxylate side chain of E562 also hydrogen bonds with

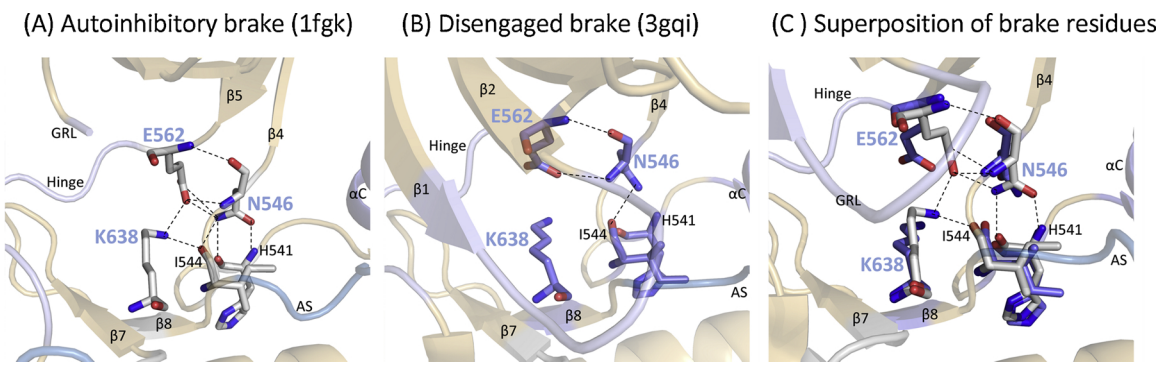

Fig. 6. (A) Hydrogen bonding pattern of the autoinhibitory brake in FGFR1. (B) Hydrogen bonding of a disengaged brake in the active form of FGFR1. (C) Superposition of the brake residues in the inactive (gray residues) and active (blue residues) forms of FGFR1. The dashed lines represent hydrogen bonds. AS, activation segment; GRL, glycine-rich loop.

the backbone N—H group of N546. Additionally, the ε-amino group of K638 and the amide side chain of N546 also form polar bonds with the carbonyl oxygen of I544 within the αC-β4 back loop. The amide and carbonyl groups of N546 also hydrogen bond with H541 within the back loop (Fig. 6A). Of the ten polar bonds observed in the autoinhibitory brake, only three are conserved in the active enzyme with a disengaged brake (Fig. 6B). The superposition of the active and inactive enzyme forms indicates that the carboxylate side chain of E562 exhibits the greatest displacement (Fig. 6C). The hydrogen bonds between N546 and the backbone atoms of H541 are critical components of the molecular brake.

1.2.3. The hydrophobic spines of FGFRs

Kornev et al. examined the arrangement of the active and inactive structures of about 20 protein kinases [21,22]. They classified four hydrophobic residues together as a regulatory or R-spine and eight hydrophobic residues together as a catalytic or C-spine (Fig. 3B/D/F). The spines extend from the N-terminal lobe into the C-terminal lobe. The R-spine contains one residue from the *α*C-helix and another from the activation segment, both components of which are key protein kinase regulatory elements. The R-spine anchors the catalytic residues in an active conformation and stabilizes the interaction of the regulatory *α*C-helix, the catalytic loop, and the activation segment while the C-spine binds ATP thus enabling catalysis. The adenine moiety of ATP is one of the components of the C-spine (Fig. 3B). Moreover, Kornev et al. [22] concluded that the accurate alignment of both spines is required for the formation of an active enzyme as described for the MEK1/2 dual specificity protein kinases [23,24], the ERK1/2 protein-serine/threonine protein kinases [25,26], the ALK receptor protein-tyrosine kinase [27,28], the EGFR family of receptor protein-tyrosine kinases [29,30], the cyclin-dependent protein-serine/threonine kinases [31,32], the Janus non-receptor protein-tyrosine kinases [33], the Kit receptor protein-tyrosine kinase [34], the Raf protein-serine/threonine protein kinases [35], the RET receptor protein-tyrosine kinase [36], the ROS1 orphan receptor protein-tyrosine kinase [37], the BTK non-receptor protein tyrosine kinase [38], the VEGFR family of receptor protein-tyrosine kinases [39], and the Src non-receptor protein-tyrosine kinase [40].

The R-spine contains (i) the first amino acid of the small lobe β4-strand, (ii) the residue that is four residues distal to the conserved αC-E residue, (iii) the phenylalanine of the DFG signature, and (iv) the histidine from the HRD signature [21]. The amide N—H group of the HRD-histidine forms a hydrogen bond with (v) the invariant aspartate carboxylate group that occurs within the αF-helix. The R-spine residues are labeled RS4, RS3, RS2, RS1, and RS0 from the top to the bottom. The R-spine of the active enzyme form is linear while the spine of the inactive DFG-D_{out} enzyme form is broken and displaced laterally (Fig. 3B and F)

Two residues of the N-terminal lobe of protein kinases interact with the adenine base of ATP; these include a conserved alanine from the AVK of the β3-strand (CS8) and a conserved valine near the beginning of the β2-strand (CS7). Furthermore, a β7-strand hydrophobic residue (CS6) from the C-terminal lobe interacts with the adenine base (Fig. 3A). The CS6 residue is next to CS5 and these residues make hydrophobic contact with the CS3 and CS4 (Fig. 3B); CS4/5/6 occur within the β7-strand and CS3 occurs near the origin of the αD-helix. CS4/5/6 can be readily identified from the primary structure because they occur immediately after the HRD(x)$_4$*N*-asparagine residue of the catalytic loop. Lastly, the CS3 and CS4 residues interact hydrophobically with CS1 and CS2 within the αF-helix thereby completing the C-spine [22]. Note that both the C-spine and R-spines are anchored by the hydrophobic αF-helix (Fig. 3D). Importantly, each spine plays an essential role in maintaining the protein kinase catalytic residues in a functional state. The most significant differences in the structures of active and inactive protein kinase spine residues usually involve the disposition of RS2 and RS3.

Meharena et al. found three protein kinase A catalytic subunit residues that strengthen the regulatory spine, which they designated as shell residues (Sh1, Sh2, and Sh3) [41]. The Sh2 residue corresponds to the gatekeeper. The amino acids that make up the C- and R-spines were identified by their location in (i) functional or in (ii) inactive protein kinases based upon their X-ray crystallographic three-dimensional structures [21,22]. This contrasts with the identification of the HRD or DFG motifs, which was based upon the conserved protein kinase primary structures [8]. The C-spine, R-spine, and shell residues of human FGFRs are listed in Table 3. Nearly all ATP-competitive protein kinase antagonists interact with CS6/7/8 of the C-spine and Sh1/2 of the shell [43].

2. Selected *FGFR* and *FGF* genomic aberrations in human cancers

2.1. An overview of urinary bladder cancers

This review focuses mainly, but not entirely, on the role of the FGFRs and FGFs in the pathogenesis of urinary bladder cancers and the treatment of these advanced or unresectable tumors by small molecule protein kinase inhibitors. The median age for the diagnosis of bladder cancer in the United States is 72 years [44]. Of the projected 80,500 cases expected in 2019, 61,500 will be diagnosed in men and 19,000 will be diagnosed in women. It is estimated that there are about 830,000 urinary bladder cancer survivors in the United States. The majority of bladder cancer survivors are men (75 %), reflecting the three-fold higher incidence of this neoplasm in males. There is considerable variation in the incidence of bladder cancer in different countries. The most common risk factor in the production of bladder cancer is cigarette smoking; the long-term effect of smoking results in the production of bladder cancer 20–40 years later. Some of the

Table 3
Human FGFR1–4 residues that form the R-spine, C-spine and Shell.

		KLIFS No.[a]	FGFR1	FGFR2	FGFR3	FGFR4
Regulatory spine						
β4-strand (N-lobe)	RS4	38	L547	L550	L541	L536
C-helix (N-lobe)	RS3	28	M535	M538	M529	M524
Activation loop (C-lobe) F of DFG	RS2	82	F642	F645	F636	F631
Catalytic loop His (C-lobe)	RS1	68	H621	H624	H615	H610
F-helix (C-lobe)	RS0	None	D682	D685	D676	D671
R-shell						
Two residues upstream from the gatekeeper	Sh3	43	V559	V562	V553	V548
Gatekeeper, end of β5-strand	Sh2	45	V561	V564	V555	V550
αC-β4 loop	Sh1	36	I545	I548	I539	I534
Catalytic spine						
β3-AxK motif (N-lobe)	CS8	15	A512	A515	A506	A501
β2-strand (N-lobe)	CS7	11	V492	V495	V486	V481
β7-strand (C-lobe)	CS6	77	L630	L633	L624	L619
β7-strand (C-lobe)	CS5	78	V631	V634	V625	V620
β7-strand (C-lobe)	CS4	76	V629	V632	V623	V618
D-helix (C-lobe)	CS3	53	L569	L572	L563	L558
F-helix (C-lobe)	CS2	None	L689	L692	L683	L678
F-helix (C-lobe)	CS1	None	I693	I696	I687	I682

[a] From Ref. [42].

differences in the incidence of bladder cancer and its variation from decade-to-decade follow changes in the previous smoking habits of the population.

More than 70 % of patients with this cancer are diagnosed with non-muscle–invasive disease (stage 0-I). For such cancers, the bladder tumor is resected transurethrally; this may be followed by intravesicular therapy with the BCG (*Bacillus Calmette-Guerin*) vaccine or intravesicular chemotherapy [45]. Although the BCG vaccine is used primarily against tuberculosis, it decreases the recurrence and slows the progression of bladder cancers; the therapeutic mechanism of this bladder cancer treatment is unclear. Mitomycin or doxorubicin (in the United States) as well as epirubicin or pirarubicin (in Europe) are intravesicular treatments that decrease recurrence. Nearly 91 % of the patients with stage I bladder cancer and about two-thirds of those with stage II disease are treated by the transurethral resection of the tumor. In contrast, about two-thirds of the patients with stage III bladder cancer receive cystectomy; this may also be followed with by chemotherapy, radiation therapy, or both.

For bladder cancers that are unresectable or that have metastasized, cisplatin-based chemotherapy is usually the first treatment option [45]. This includes the combination of (i) methotrexate, vinblastine, doxorubicin (Adriamycin), and cisplatin (M-VAC), (ii) cisplatin, methotrexate and vinblastine (CMV), or (iii) gemcitabine, cisplatin, and paclitaxel (GCP). Five immune checkpoint inhibitors have been FDA-approved for the treatment of metastatic bladder cancer [45,46]. These include nivolumab and pembrolizumab that target PD-1 and atezolizumab, avelumab, and durvalumab that target PD-L1. PD-1 refers to the transmembrane programmed cell death protein-1 (also known as CD279) and PD-L1 (CD274) refers to its ligand. Erdafitinib is a FGFR inhibitor that has been approved for the treatment of metastatic bladder cancer [47].

2.2. FGFR and FGF gene alterations in urinary bladder cancer

Several *FGFR1/2/3/4* gene alterations have been described in bladder cancers (Table 4) [1]. The *FGFR1* alterations include *FGFR1* amplification and a T141R mutation near the extracellular D2 domain (Table 5) [48]. *FGFR* gene amplification is generally associated with overexpression of the gene product leading to increased enzyme activity. A translocation resulting in a *FGFR1-NTM* chimeric fusion protein also occurs [48]. The *FGFR* gene fusion partner leads to the dimerization of the chimeric protein and its subsequent activation. A FGFR2-TACC3 fusion protein has been observed in bladder cancers. Moreover, *FGFR3* gene amplification can also produce bladder cancer. Furthermore, several mutations within the extracellular domain of *FGFR3* have been described: S131L, R248C, S249C, G370C, Y373C. The conversion of an extracellular residue to cysteine may promote the formation of an aberrant disulfide bond leading to the formation of an adventitious receptor dimer resulting in transphosphorylation and kinase activation. Two mutations within the intracellular domain have been reported: K650 M (activation segment) and G818R (carboxyterminal tail). Moreover, *FGFR3* mutations occur in more than one-half of all non-muscle–invasive urinary bladder cancers and in about 10 % of the more severe muscle-invasive urinary bladder cancers [49]. Four FGFR3 chimeras have been described including *FGFR3-TACC3, FGFR3-JAKMIP*, *FGFR3-TNIP2*, and *FGFR3-ADD1* (Table 5). The FGFR fusion protein partner generally leads to receptor dimerization and subsequent protein kinase transphosphorylation and activation.

Besides the FGFRs, numerous *FGF* gene alterations have been described in various cancers (Table 6). The most commonly involved factors among all of the neoplasms are FGF3/4/19. Again, gene alterations in urothelial bladder cancers are among the most prevalent with FGF3/4/19 being co-amplified in about 12 % of cases [1]. Amplification generally results in overproduction of these factors and an increase in FGF signaling. In contrast, gene alterations involving FGF17 and FGF20 in urinary bladder cancers are mostly deletions, which result in decreased growth factor signaling. Thus, the mechanism for the production of urothelial cancers that result from FGF alterations differs among the various factors. In some cases increased action and in other cases decreased activity promote the neoplastic state.

2.3. Selected FGFR and FGF genomic alterations in other human cancers

Helsten et al. analyzed the frequencies of *FGFR* aberrations in more than 4800 solid tumors using next-generation DNA sequencing [48]. They reported that such aberrations occurred in 7.1 % of all of their cancer specimens. The majority (66 %) of gene alterations in their study involve gene amplifications, followed by mutations (26 %), and finally translocations or gene rearrangements (8 %). Their data indicate that the frequency of *FGFR1* alterations (mostly amplifications) in the 4800-patient cohort was 3.5 %, that of *FGFR2* was 1.5 %, that of *FGFR3* was 2.0 %, and that of *FGFR4* was 0.5 %. Nearly all of the various malignancies that they analyzed exhibited *FGFR* alterations. The most commonly affected neoplasms include urothelial carcinomas (aberrations in 32 % of all urothelial carcinomas), breast cancers (18 %), endometrial cancers (13 %), squamous cell lung cancers (13 %), ovarian cancers (9 %), gliomas (8 %), cholangiocarcinomas (7 %), sarcomas (4 %), lung adenocarcinomas (4 %) and colorectal, neuroendocrine, pancreatic, and renal cancers (4 %–5 % each).

Amplification of *FGFR1* is a predominant abnormality that leads to the production of several commonly occurring tumors including squamous cell carcinomas of the lung and breast [49]. Gene amplification has also been described in ovarian (*FGFR1/2/3*) and bladder carcinomas (*FGFR1*/3) as well as gliomas (*FGFR3*) and sarcomas (*FGFR1/2*) (Table 5) [49,50]. Such amplifications are generally diagnosed using fluorescence in situ hybridization (FISH); however, cut-off values for a definition of *FGFR* amplification are still undetermined. In contrast to gene amplification as a causative agent, *EGFR* gene mutations lead to the production of many lung cancers [30]. Moreover, $BRAF^{V600E/K}$ mutations, but not *BRAF* amplification, are responsible for the production of melanomas [35]. Similarly, *Kit* mutations occur in a variety of diseases including gastrointestinal stromal tumors, mastocytosis, core-binding factor acute myelogenous leukemia, and seminomas [34]. With the exception of *ErbB2/HER2* amplification in breast cancers [30], gene amplification of protein-tyrosine kinase receptors (*FGFR1/2/3/4*)

Table 4
Selected fibroblast growth factor receptor genomic alterations in human cancers[a].

Type of cancer	Approximate prevalence[c]	Approximate frequencies by FGFR[b]			
		FGFR1	FGFR2	FGFR3	FGFR4
Urothelial bladder cancers	35 %	14 %	3 %	19 %	6 %
Squamous cell lung carcinomas	27 %	18 %	4 %	4 %	2 %
Uterine endometrial carcinomas	24 %	7 %	14 %	5 %	4 %
Gastric adenocarcinomas	23 %	6 %	10 %	4 %	5 %
Breast adenocarcinomas	20 %	14 %	3 %	2 %	2 %
Melanomas	20 %	5 %	11 %	5 %	5 %
Ovarian serous cystadenocarcinomas	20 %	5 %	4 %	8 %	4 %
Head & neck squamous cell carcinomas	17 %	10 %	1 %	4 %	1 %
Lung adenocarcinomas	14 %	6 %	4 %	2 %	4 %
Prostate adenocarcinomas	11 %	6 %	3 %	1 %	1 %
Colorectal adenocarcinomas	8 %	5 %	1 %	1 %	1 %
Cholangiocarcinomas	7 %	0.9 %	6.1 %	0 %	0 %
Glioblastomas	6 %	0 %	3 %	2 %	1 %
Lower grade brain gliomas	5 %	0 %	3 %	1 %	1 %

[a] Data from Ref. [1].
[b] Most of the studies included > 200 cases; analyses performed in 2014; values may not add up to approximate prevalence owing to rounding errors.
[c] Prevalence among all analyses performed on each particular neoplasm.

as the main causative agents of a variety of neoplasms represents an unusual situation.

About 8 % of *FGFR* genetic alterations that produce neoplasms are due to the production of FGFR fusion proteins or chimeras [48]. Various fusion partners include TACC1/2/3, BAIAP2L1, NPM1, AFF3, BICC1, NOL4, and KIAA1579 [48,51–53]. The transforming acidic coiled-coil containing protein gene-3 (TACC3) was first identified as a component of the FGFR3-TACC3 fusion protein in urothelial bladder cancers and in glioblastoma multiforme. This fusion protein, which is the most common of the FGFR chimeras, is constitutively active and it alters chromosomal segregation. Most of the gene alterations that produce cholangiocarcinomas are caused by the formation of *FGFR2* fusion protein chimeras [48]. A variety of point mutations of all four receptors have been described [48,51]. These occur in the extracellular domains and the transmembrane segments of FGFR1/2/3, the activation segments of FGFR1/3, and the asparagine brake residues of FGFR1/2 (Table 5). Approximately 15–20 % of patients with multiple myeloma overexpress FGFR3 as a consequence of a t(4;14)(p16.3;q32) translocation [54,55]. This translocation brings FGFR3 under the influence of a strong immunoglobulin H enhancer thereby leading to FGFR3 overexpression.

A variety of cancers in addition to those of the bladder result from *FGF* gene alterations (Table 6). Alterations of *FGF3/4/19/12/10/23* genes occur frequently in head and neck squamous cell carcinomas and virtually all of these are related to gene amplification. There is also a high incidence of *FGF3/4/19/10/12/13/14/17* gene alterations in gastric cancers; FGF3/4/19 are co-amplified in about 7 % of these cases. *FGF* alterations in cervical (*FGF10*) and ovarian (*FGF3/4/19/6/23/12*) cystadenocarcinomas are almost all due to gene amplification. Moreover, *FGF3/4/19/12/10* gene mutations in squamous cell lung carcinomas and *FGF10/17/20* gene mutations in lung adenocarcinomas occur frequently with almost no overlap except for *FGF10*. There is a high prevalence of *FGF3/4/19* gene amplification in melanomas and these three genes are co-amplified in about 7 % of cases. Helsten et al. reported that *FGF* gene anomalies occur in about 14 % and *FGFR* gene alterations occur in about 7 % of all malignancies [1]. In summary, there are a large number of *FGFR* and *FGF* gene alterations that are involved in the pathogenesis of several commonly occurring cancers.

3. Protein kinase inhibitor classification

In an initial classification, Dar and Shokat divided small molecule protein kinase inhibitors into groups I, II, and III [56]. Type I antagonists bind within and near the adenine-binding site of a protein kinase in its active DFG-D_{in} conformation. Type II inhibitors, in contrast, bind to the non-functional DFG-D_{out} protein kinase conformation while type III inhibitors bind to an allosteric site in an active or inactive conformation that does not preclude ATP binding. Expanding on these definitions, type I½ inhibitors are antagonists that bind to a non-functional enzyme with a DFG-D_{in} structure [16]. Such an inactive protein kinase may display a closed activation segment (Fig. 3C), an abnormal glycine-rich loop, a non-linear R-spine (Fig. 3F), an αC_{out} conformation, an autoinhibitory brake, or various combinations of these structures. Additionally, Gavrin and Saiah subdivided allosteric inhibitors into types III and IV [57]. Their type III inhibitors bind within the cleft between the N-terminal and C-terminal lobes without overlapping the ATP binding pocket. Their type IV inhibitors, in contrast, bind outside of the region between the two lobes. Furthermore, Lamba and Gosh named compounds that span two portions of the protein kinase domain type V, or bivalent, inhibitors [58]. For example, an antagonist that binds to (i) the adenine site of an enzyme such as Src and (ii) its SH2 domain is considered to be a type V inhibitor [59]. We subsequently named type VI inhibitors as those antagonists that form a covalent bond with their target enzyme [60]. Afatinib is an example of a covalent Type VI inhibitor that is used for the treatment of NSCLC bearing an *EGFR* mutation [43]. This antagonist binds initially as a type I inhibitor to an active EGFR conformation (PDB ID: 4g5j); afterwards the C797 –SH group of the protein attacks the antagonist forming a stable covalent Michael adduct [60].

We previously divided type I½ and type II pharmaceuticals into A and B subtypes [60]. Type A inhibitors such as sorafenib are agents that extend past the gatekeeper into the hydrophobic back cleft. In contrast, type B inhibitors are antagonists that do not extend into this back cleft. The potential significance of this distinction is that type A inhibitors bind to their target enzyme with a longer residence time [61] when compared with type B inhibitors [60]. Sorafenib is a VEGFR type IIA therapeutic that is FDA-approved for the treatment of renal cell carcinomas. Sunitinib is a VEGFR type IIB inhibitor that is also FDA-approved for the treatment of these carcinomas. The type IIA inhibitor has a residence time of greater than 64 min while that of the type IIB inhibitor has a residence time of less than 2.9 min [60].

4. Drug-ligand binding pockets

Liao [62] and van Linden et al. [42] divided the section between the N-terminal and C-terminal lobes of protein kinases into a front cleft (front pocket), a gate area, and a back cleft. Hydrophobic pocket II (HPII) consists of the gate area and back cleft (Fig. 7). The front cleft

Table 5
Selected FGFR alterations in cancer.

Malignancy	Gene alteration[a]	Location
Urothelial bladder cancers	*FGFR1* amplification	
	FGFR1-T141R	Acid box–D2 linker
	FGFR1-NTM chimera	
	FGFR2-TACC3 chimera	
	FGFR3 amplification	
	FGFR3-131L	Before the acid box
	FGFR3 R248C	D2–D3 linker
	FGFR3 S249C	D2–D3 linker
	FGFR3-G370C	Before the transmembrane segment
	FGFR3 Y373C	Before the transmembrane segment
	FGFR3 K650M	Activation segment
	FGFR3 G818R	Carboxyterminal tail
	FGFR3-TACC3 chimera	
	FGFR3-JAKMIP chimera	
	FGFR3-TNIP2 chimera	
	FGFR3-ADD1 chimera	
Breast cancers	*FGFR1* amplification	
	FGFR2 amplification	
	FGFR2 S252W	D2–D3 linker
	FGFR2-NCALD chimera	
	FGFR3-WHSC1	
	FGFR4 amplification	
Endometrial uterine cancers	*FGFR2* amplification	
	FGFR1 T141R	Acid box
	FGFR2 P253R	D2–D3 linker
	FGFR2 C382R	Transmembrane segment
	FGFR2-N549 K	"αC-β4 loop brake residue"
	FGFR2-V677I	Activation segment-αF loop
Lung cancers	*FGFR1* amplification	
	FGFR1 T141R	Acid box–D2 linker
	FGFR2 A315C	D3
	FGFR3 amplification	
	FGFR3 R248C	D2–D3 linker
	FGFR3 S249C	D2–D3 linker
	FGFR3 G370C	Before transmembrane segment
	FGFR3 K560E	Hinge
	FGFR4 amplification	
	FGFR4 R183S	D2
Ovarian cancers	*FGFR1* amplification	
	FGFR2 amplification	
	FGFR2 S252W	D2–D3 linker
	FGFR3 amplification	
Stomach cancers	*FGFR1* amplification	
	FGFR2 amplification	
	FGFR2-TACC2 chimera	
	FGFR3 amplification	
	FGFR3 R399C	Intracellular juxtamembrane segment
Cholangiocarcinomas	*FGFR2* amplification	
	FGFR2 C382R	Transmembrane segment
	FGFR2-NOL4	
	FGFR2-KIAA1579	
	FGFR2-BICC1	
	FGFR2-TACC3	
Gliomas	*FGFR1 N546K*	αC-β4 loop brake residue
	FGFR1-K656E	Activation segment
	FGFR3 amplification	
	FGFR3 K650E	Activation segment
	FGFR3-TACC3 chimera	
Sarcomas	*FGFR1* amplification	
	FGFR1 N546K	αC-β4 loop brake residue
	FGFR2 amplification	
	FGFR2 N549 K	αC-β4 loop brake residue
	FGFR3 R248C	D2–D3 linker
	FGFR3 E627K	β6-β7 loop

[a] Data from Ref. [48].

Table 6
Selected fibroblast growth factor genomic alterations in human cancers[a].

Type of cancer	Approximate prevalence [c]	Approximate (%) prevalence by FGF[b]
Head & neck squamous cell carcinomas	54 %	FGF3/4/19/12/10/23 (28/28/28/19/6/5)
Urothelial bladder cancers	47 %	FGF3/4/19/17/10/20 (13/12/13/11/9/9)
Gastric cancers	47 %	FGF3/4/19/10/12/13/14/17 (7/7/7/9/8/6/5/5)
Lung, squamous cell carcinomas	46 %	FGF3/4/19/12/10 (12/12/13/25/7)
Cervical cancers	42 %	FGF12 (25)
Lung, adenocarcinomas	39 %	FGF10/17/20 (11/7/7) [d]
Melanomas	38 %	FGF3/4/19 (8/6/6)
Ovarian cystadenocarcinomas	38 %	FGF3/4/19/6/23/12 (5/4/4/5/6/13)
Breast adenocarcinomas	35 %	FGF3/4/19/17/20 (15/15/15/6/5) [e]
Adenoid cystic carcinomas	27 %	FGF22 (10) all others 5 % or less
Prostate adenocarcinomas	22 %	FGF17/20 (8/5) [f]
Colorectal adenocarcinomas	17 %	All 5 % or less [g]

[a] Data from Ref. [1].
[b] Most of the studies included at least five cases with the alteration; analyses performed in 2014; values may not add up to approximate prevalence owing to high frequency of duplicate-triplicate changes in a single sample and to rounding errors.
[c] Prevalence among all analyses performed on each particular neoplasm; most alterations are due to gene amplification.
[d] FGF17/20 mostly deletions.
[e] High frequency of FGF3/4/19 co-amplification.
[f] Majority are deletions.
[g] Majority are mutations.

consists of the hinge residues along with the adjacent adenine-binding pocket (AP), the residues of the catalytic loop (HRD(x)$_4$N), and the glycine-rich loop. The gate area consists of the small lobe β3-strand and the proximal portion of the large lobe activation segment including DFG. The back cleft consists of the small lobe αC-β4 back loop and the β4- and β5-strands and the large lobe αE-helix. Designing pharmaceuticals to interact with residues lining the various binding pockets plays an important role in protein kinase antagonist development with a strategy aimed at maximizing drug affinity.

van Linden et al. described several front pocket, gate area, and back cleft regions (Table 7) [42]. Accordingly, the front cleft contains residues that constitute the adenine-binding pocket (AP) as well as two nearby front pockets (FP-I and FP-II). Most ATP-competitive steady-state inhibitors possess a core pharmacophoric platform that interacts with essential features of the adenine binding site. This core scaffold is linked to various chemical fragments that interact with nearby binding pockets or subpockets. FP-I resides between the C-terminal lobe xDFG (x is the amino acid residue immediately preceding the activation loop DFG signature sequence) and the hinge residues exposed to the solvent and FP-II occurs between the glycine-rich loop and the N-terminal lobe β3-strand near the ceiling of the cleft. BP-I-A and BP-I-B are found in the gate area between the β3- and β4-strands, the αC-helix, the N-terminal lobe β3-strand K of the AxK signature, and the C-terminal lobe xDFG-motif. The smaller BP-I-A compartment, which is found near the uppermost gate area, is enclosed by residues of the β5- and adjacent β3-strands including the AVK signature residues and the αC-helix. The larger BP-I-B occurs in the central gate area and allows for access to the back cleft. Both BP-I-A and BP-I-B are found in both the DFG-D_{in} and the DFG-D_{out} protein kinase configurations.

BP-II-in and BP-II-A-in are found within the back cleft of the DFG-D_{in} protein kinase conformation [62]. These pockets are bounded by the N-terminal lobe αC-helix, the αC-β4 back loop, and the β5- and β4-

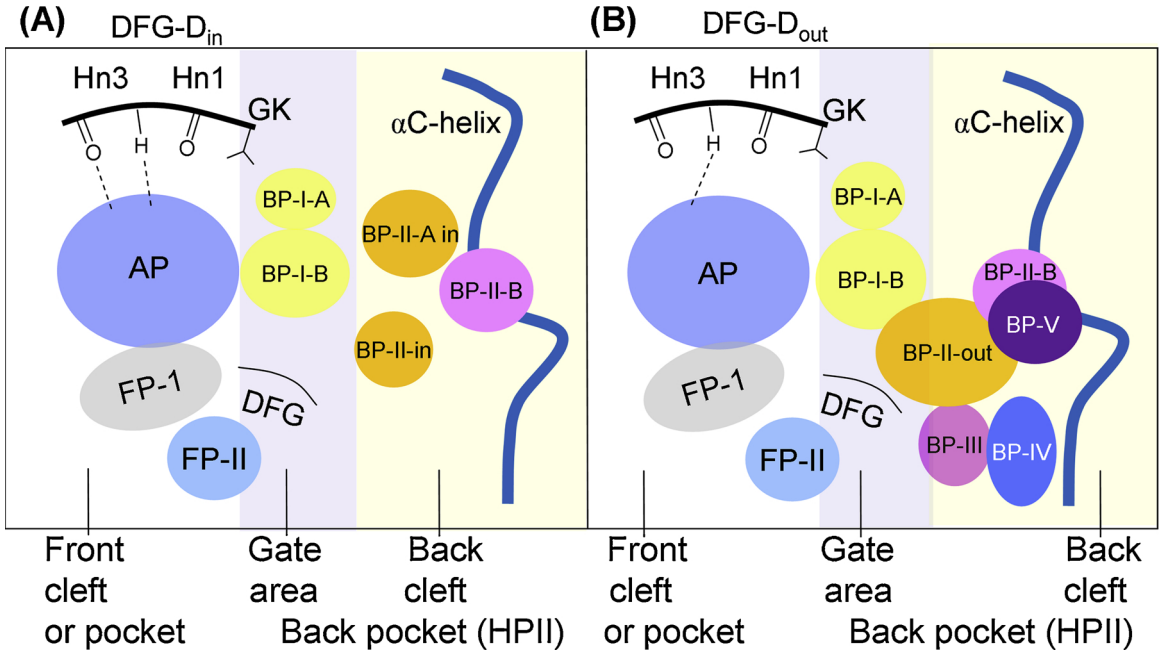

Fig. 7. Location of the protein kinase domain drug-binding pockets. AP, adenine pocket; BP, back pocket; FP, front pocket; Hn, hinge; HPII, hydrophobic pocket II; GK, gatekeeper. Adapted from Refs. [42,62].

Table 7
Location of selected catalytic cleft residues.

Description	Location	KLIFS residue no.[a]
GxGxΦG	Front cleft	4–9
β2-strand V (CS7)	Front cleft	11
β3-strand A (CS8)	Front cleft	15
HRD with DFG-D_{in}	Front cleft	68–70
$HRD(x)_4N$-N	Front cleft	75
β7-strand CS6	Front cleft	77
β3-strand K; three residues before the αC-helix	Gate area	17
αC-β4 penultimate back loop residue	Gate area	36
Gatekeeper	Gate area	45
The x of xDFG	Gate area	80
DFG	Gate area	81–83
αC-helix E	Back cleft	24
RS3	Back cleft	28
HRD with DFG-D_{out}	Back cleft	68–70

[a] Ref. [42].

strands and the C-terminal lobe DFG-signature. Key conformational changes of BP-II-in and BP-II-A-in generate the BP-II-out compartment that exists only in the DFG-D_{out} conformation; these structural changes are a result of the movement of DFG-F. This interchange brings about the formation of BP-II-out; it occupies the space where the DFG-F is found in the DFG-D_{in} structure. BP-II-B is bounded by the αC-helix and the nearby β4-strand in both the DFG-D_{in} and DFG-D_{out} configurations. In contrast to BP-II-B, BP-III occurs only in the DFG-D_{out} structure (Fig. 3B). BP-III is found on the floor of the BP-II-out pocket between the αC-β4 back loop, the αC-helix of the small lobe, the β6-strand residues, the αE-helix, the activation segment DFG-D_{out} signature sequence, and the conserved catalytic loop HRD-H of the large lobe. BP-IV and BP-V, which are partially solvent exposed, are found between the β6-strand residues, the catalytic loop, the DFG-D_{out} motif and the activation segment of the large lobe and the small lobe αC-helix (Fig. 7).

van Linden et al. created a comprehensive catalog of structures depicting drug and ligand binding to more than 1200 human and mouse protein kinases [42]. Their KLIFS (kinase–ligand interaction fingerprint and structure) formulary includes an array of 85 possible ligand binding-site residues that occur in both the small and large lobes. Their catalog aids in the discovery of correlated interactions and facilitates the classification of pharmaceuticals based upon their binding features. Furthermore, this consortium devised a common amino acid residue numbering convention that aids in the comparison of different drug-kinase interactions. The correspondence between the KLIFS catalog of residue numbers and the FGFR R-spine, shell, and C-spine amino acid residue nomenclature is provided in Table 3. Additionally, this consortium launched an informative non-commercial searchable web site, which is regularly updated, that describes the interaction of protein kinases with ligands and drugs (klifs.vu-compmedchem.nl/). Moreover, Carles et al. devised a comprehensive directory of small molecule protein kinase and PI3K blockers that have been or are being studied in clinical trials [63]. These investigators launched a non-commercial searchable web site, which is also regularly updated, that includes inhibitor structures and physicochemical properties, their enzyme and therapeutic targets, and their trade names (http://www.icoa.fr/pkidb/). Furthermore, the BRIMR (Blue Ridge Institute for Medical Research) website, which is also regularly updated, provides the structures and Lipinski rule of five properties [64] of all FDA-approved small molecule protein kinase inhibitors (www.brimr.org/PKI/PKIs.htm).

5. Structure of FGFR-drug complexes

5.1. Erdafitinib

Erdafitinib is a quinoxaline derivative (Fig. 8A) [65] that was approved for the first-line treatment of urothelial bladder cancer bearing susceptible *FGFR2/3* mutations or for the second-line treatment of locally advanced or metastatic bladder cancer following platinum-based chemotherapy (Table 8) [47]. Importantly, urothelial cancers are the fourth most prevalent cancer worldwide and erdafitinib fulfills an unmet medical need. Moreover, erdafitinib was granted accelerated approval by the FDA. Such designations indicate that additional ongoing clinical trials will be necessary to confirm the clinical benefit of this medication. The response rate of erdafitinib therapy in the second-line treatment of patients with *FGFR3* mutations or *FGFR2/3* fusion proteins was 40 % with 3 % achieving a complete response and 37 % achieving a partial response [66]. The IC_{50} values for FGFR1/2/3/4 are 2.0/2.0/4.0/6.3 nM and that for VEGFR2 is 50 nM. Erdafitinib is a potent inhibitor of all of the fibroblast growth factor kinases and is classified as a pan-FGFR inhibitor (Table 9).

The X-ray crystal structure of erdafitinib bound to FGFR1 shows that the *N*1 of quinoxaline forms a hydrogen bond with A564 (the third hinge residue) and the dimethoxyphenyl oxygen forms a hydrogen bond with the N−H group of DFG-D641 (Fig. 9A) [51]. Erdafitinib makes hydrophobic contact with five spine residues (RS2/3, CS6/7/8) and all three shell residues (Sh1/2/3) (Table 10). The pharmaceutical interacts hydrophobically with the β1-strand residue immediately preceding the glycine-rich loop (L484); this residue corresponds to KLIFS-3 (kinase–ligand interaction fingerprint and structure residue-3). Erdafitinib also makes hydrophobic contact with AVK514 of the β3-strand, I545 of the αC-β4 back loop, E562,Y563, A564, and S565 within the hinge, as well as $HRD(x)_4N628$, and A640 (the x of xDFG). The therapeutic occupies the front cleft, the gate area, and the back cleft including FP-I, BP-I-A, and BP-I-B and it extends past the gatekeeper residue. The compound is bound to a DFG-D_{in} inactive conformation of FGFR1 with the autoinhibitory brake and the activation segment in a closed conformation. Overall this interaction corresponds to that of a type I½A inhibitor [60].

One of the most common side effects of erdafitinib is hyperphosphatemia, which occurs in about three-quarters of patients [47,66]. As noted in Table 1, FGF23 participates in the regulation of phosphate homeostasis. Under physiological conditions, FGF23 released from the bone suppresses phosphate reabsorption in the proximal tubules of the kidney [67]. Blockade of the action of FGF23 allows phosphate reabsorption and this leads to hyperphosphatemia; it appears that FGFR1 is a major participant in renal phosphate homeostasis [68,69], although this is not entirely settled and it may also involve the participation of FGFR3/4 [70]. Chronic elevated serum phosphate may lead to ectopic calcification in soft tissues. Serum phosphate represents a biomarker for the inhibition of FGFRs and it is class specific reflecting inhibition of FGF23 action and not that of other growth factors or their corresponding receptor protein kinases. Grade 3 (out of 4) hyponatremia occurs in about 11 % of patients [66]; the mechanism of this response is unclear. See Refs [47,71]. for a summary of the clinical trials that led to the approval of erdafitinib.

5.2. Ponatinib

Ponatinib is an imidazo[1,2-*b*]pyridazine derivative (Fig. 8B) [72] that is FDA-approved for the treatment of Philadelphia chromosome positive CML and ALL (Table 8). See Refs. [73,74] for a summary of the clinical trials that led to these approvals. Huang et al. initially developed this pharmaceutical as a BCR-Abl non-receptor protein-tyrosine kinase inhibitor with activity against the *Abl* T315I gatekeeper mutation [74]. The IC_{50} values for FGFR1/2/3/4 are 2.2/1.6/18.2/7.7 nM, those for VEGFR1/2/3 are 3.7/1.5/2.3 nM, those for PDGFRα/β are 1.1/7.7 nM, that for RET is 0.2 nM, that for Kit is 12.5 nM, that for CSF1R is 8.6 nM, and that for Flt3 is 12.6 nM [75]. Based on these data, ponatinib is classified as a multi-kinase inhibitor (Table 9). The therapeutic is in clinical trials for tumors that have increased FGFR activity. The X-ray crystal structure of ponatinib bound to human FGFR4 as determined by Tucker et al. (4uxq) [76] demonstrates that the

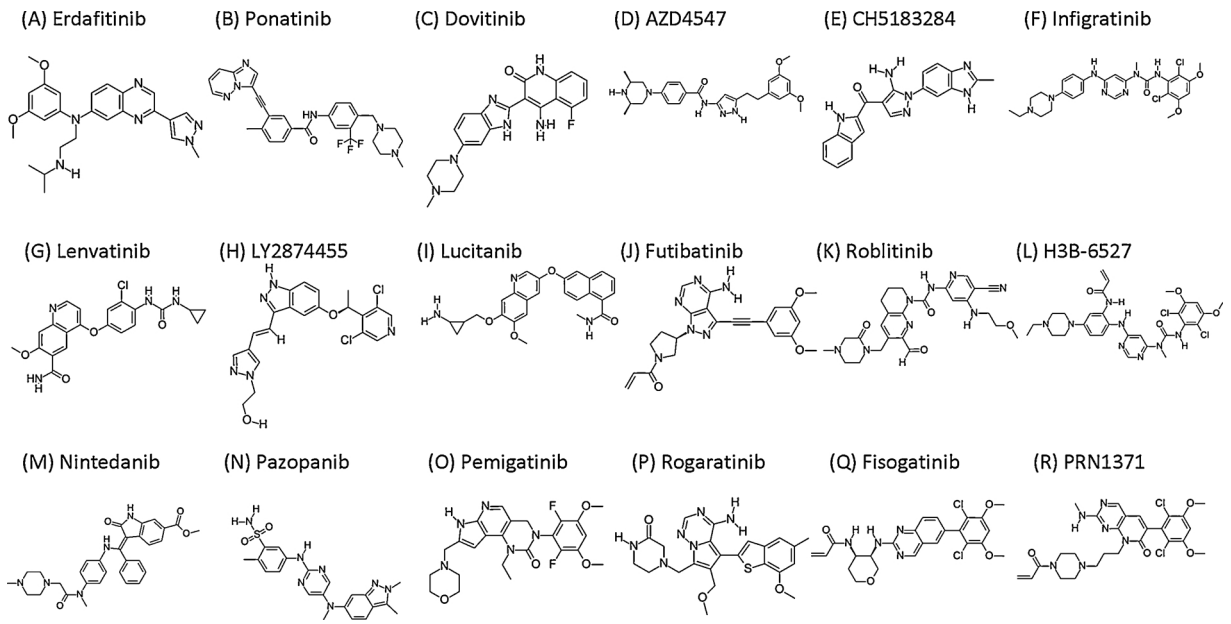

Fig. 8. Structures of selected fibroblast growth factor receptor inhibitors.

imidazopyridazine scaffold forms a hydrogen bond with the A553 N—H group (the third hinge residue) of FGFR4 (Fig. 9B). An amino N—H group from the pharmaceutical forms a hydrogen bond with the side chain carboxylate group of E520 within the αC-helix, the pharmaceutical carbonyl oxygen forms a hydrogen bond with the N—H group of DFG-D630, and the piperazinyl nitrogen forms a hydrogen bond with the carbonyl oxygen of I609; I609 occurs immediately before the HRD-H610. Ponatinib makes apolar contact with six spine residues (RS1/2/3, CS6/7/8), all three shell residues (Sh1/2/3), and the KLIFS-3 residue. The therapeutic makes hydrophobic contact with the β3-strand V502, the αC E520, V523, and M524, the αC-β4 back loop I527, the β6-strand C608 and I609. It also makes hydrophobic contact with the catalytic loop R611, the β8-strand I628 and A629 (the x of xDFG). Because the ligand extends past the gate area of the DFG-D_{out} structure, the overall classification is that of a Type IIA inhibitor [60]. Ponatinib has not been shown to increase serum phosphate levels.

Lesca et al. [77] and Huang et al. [78] also determined the X-ray crystal structure of ponatinib bound to FGFR4 (PDB ID: 4tyj and 4qrc, respectively). The FGFR4 DFG-D_{out} structures from these two studies were superimposable with each other with the exception of a portion of the activation segments (not shown). The hydrogen bonding patterns were the same in these two studies except that the 4qrc structure had an additional bond from the piperazinyl nitrogen to the carbonyl group of the HRD-H610. All three of the aforementioned ponatinib-FGFR4 structures exhibit the characteristics of a Type IIA inhibitor and ponatinib occupies the front cleft, gate area, back cleft, BP-I-A/B, BP-II-out, BP-III, and BP-IV (Table 10).

5.3. Dovitinib

Dovitinib is a quinoline-benzimidazole derivative (Fig. 8C) that is in several clinical trials targeting various solid tumors including those of the bladder (Table 8). The IC_{50} values for FGFR1/2/3/4 are 10/400/3.2/3000 nM, those for VEGFR1/2/3 are 3.2/20/2.5 nM, those for PDGFRα/β are 50/4 nM, that for Kit is 1 nM, and that for RET is 5.0 nM (ChEMBL ID: CHEMBL522892). Based on these findings, dovitinib is classified as a multi-kinase inhibitor (Table 9). Bunney et al. and Klein et al. described the X-ray crystal structure of the pharmaceutical bound to FGFR1 [79,80]. The quinoline N—H group hydrogen bonds to the carbonyl group of E562 (the first hinge residue) and the 2-keto group of the quinoline scaffold hydrogen bonds with the N—H group of A564 within the hinge; moreover, an N—H group from the benzimidazole hydrogen bonds with the carbonyl group of A564 (Fig. 9C). Moreover, dovitinib makes hydrophobic contact with three spine residues (CS6/7/8), two shell residues (Sh1/2), and KLIFS-3. The therapeutic also interacts hydrophobically with AVK514 and E562, Y563, A564, S565, and K566 of the hinge. Dovitinib binds to residues within the front pocket and does not extend past the gatekeeper residue. The enzyme exists in a DFG-D_{in} inactive conformation with the autoinhibitory brake and a closed activation segment. The dovitinib-FGFR1 exhibits the properties of a Type I½B inhibitor [60]. Dovitinib binds to the gatekeeper V561 M mutant (PDB ID: 5am7) as described for the wildtype enzyme (PDB ID: 5am6). However, there is greater hydrophobic interaction of the drug with the mutant M561residue than with the wild type V561 residue. Unlike erdafitinib, dovitinib fails to produce hyperphosphatemia [67].

5.4. AZD4547

AZD4547 is a pyrazole derivative (Fig. 8D) that is an inhibitor of FGFR1/2/3 (IC_{50} values of 0.2/1.8/2.5 nM) with weaker activity against FGFR4 (IC_{50} value of 165 nM) and VEGFR2 (IC_{50} value of 24 nM) [75]. It also inhibits CSF1R (IC_{50} of 9.7 nM), Kit (24 nM), and Flt3 (85 nM). Based on these data, AZD4547 is classified as a FGFR1/2/3 inhibitor (Table 9). It is in several clinical trials that are directed toward a variety of solid tumors (Table 8). Tucker et al. and Sohl et al. determined the X-ray crystal structure of AZD4547 bound to FGFR1 [76,81]. The structures show that the pyrazole group forms hydrogen bonds with the carbonyl group of E562 and the N—H group of A564 of the hinge (Fig. 9D). An amino group from the pharmaceutical forms another hydrogen bond with the carbonyl group of A564. Furthermore, an oxygen atom from one methoxy group forms a hydrogen bond with the N—H group of DFG-D641. The pharmaceutical makes apolar contact with five spine residues (RS2/3, CS6/7/8), three shell residues (Sh1/2/3), and KLIFS-3 (Table 10). Moreover, it interacts hydrophobically with F489 within the glycine-rich loop (the Φ of GxGxΦG), AVK-K514 within the β3-strand, E531 and M535 within the αC-helix, I545 within the αC-β4 back loop, Y563, A564, S565, and K566 within the hinge, E571 within the αD-helix, A640 (the x of xDFG), and DFG-D641. AZD4547 occupies the front cleft, gate area, and back cleft including BP-I-A and BP-I-B and it extends past the gatekeeper residue. The drug binds to an inactive (autoinhibited brake, closed activation segment) DFG-D_{in} enzyme form and is classified as a Type I½A inhibitor [60]. Like

Table 8
Properties of selected orally effective small molecule FGFR family inhibitors.

Name (code) trade name	Targets	PubChem CID[a]	Formula	D/A[b]	MW (Da)	c Log P	Hyper Pi[c]	FDA-approved indications (year) or clinical trial studies (clinicaltrials.gov)[d]
Reversible inhibitors with drug-FGFR X-ray crystal structures								
Erdafitinib (JNJ-42756493) Balversa	FGFR1/2/3/4, VEFGR2	67462786	$C_{25}H_{30}N_6O_2$	1/7	446	3.2	Yes	First-line FGFR mutant urinary bladder cancers (2019); second-line metastatic or unresectable urinary bladder cancers (2019). A total of 18 clinical trials targeting HCC, breast cancers, lymphomas, multiple myelomas.
Ponatinib (AP24534) Iclusig	FGFR1/2/3/4, Abl, PDGFα/β, RET, Kit, CSF1R, Flt3, VEGFR1/2/3	24826799	$C_{29}H_{27}F_3N_6O$	1/8	533	4.1	No	Philadelphia chromosome positive CML and ALL (2012). A total of 57 clinical trials including 2 targeting FGFR dysregulation. Other targets include head & neck cancers and NSCLC.
Dovitinib (CHIR 258, TKI 258)	FGFR1/3, VEGFR1/2/3, PDGFRβ, Kit, RET	135398510	$C_{21}H_{21}FN_6O$	3/6	392	1.6	No	A total of 48 trials targeting multiple myeloma and solid tumors including urinary bladder cancer, GIST, kidney, stomach, adrenal cortical, colorectal, pancreatic, breast, prostate, thyroid, hepatic, and head & neck cancers, NSCLC, and glioblastoma
(AZD4547)	FGFR1/2/3/, VEFGR2, CSF1R, Kit	51039095	$C_{26}H_{33}N_5O_3$	3/6	464	3.9	Yes	A total of 15 clinical trials targeting NSCLC, squamous cell lung, breast, stomach, and bladder cancers, lymphomas, and myelomas.
(CH5183284; Debio 1347)	FGFR1/2/3	66555680	$C_{20}H_{16}N_6O$	3/4	356	3.9	Unkn	A total of 3 trials targeting breast cancer and advanced solid tumors.
Infigratinib (BGJ398)	FGFR1/2/3	53235510	$C_{26}H_{31}Cl_2N_7O_3$	2/8	561	4.7	Yes	Of 15 trials, a total of 6 are examining FGFR dysregulation including those targeting advanced solid tumors, cholangiocarcinomas, and head & neck carcinomas.
Lenvatinib (E7080) Lenvima	FGFR1/2/3, VEGFR1/2/3, RET, Kit	9823820	$C_{21}H_{19}N_4ClO_4$	3/5	427	2.8	No	Differentiated thyroid cancers (2015). A total of 121 clinical trials for advanced solid tumors, HCC, RCC, melanomas, breast cancers, sarcomas, thyroid cancers, endometrial cancers, and rectal cancers; one trial examining FGFR dysregulation in advanced cancers.
(LY2874455)	FGFR1/2/3/4	46944259	$C_{21}H_{19}Cl_2N_5O_2$	2/5	444	3.5	Yes	Only 2 clinical trials (AML and advanced cancers) with the latter examining FGFR dysregulation (NCT01212107).
Lucitanib (E-3810)	FGFR1, VEGFR1/2, PDGFRα/β,Src	25031915	$C_{26}H_{25}N_3O_4$	2/6	444	3.6	No	A total of 31 trials targeting solid tumors, breast cancer, gastric or duodenal ulcers, and dyspepsia with 3 trials targeting FGFR genetic alterations.
Irreversible inhibitors with drug-FGFR X-ray crystal structures								
Futibatinib (TAS-120)[e]	FGFR1/2/3/4	71621331	$C_{22}H_{22}N_6O_3$	1/7	418	2	Yes	Of 4 clinical trials, two are directed against FGFR2 dysregulation in metastatic breast cancer and cholangiocarcinomas.
Roblitinib (FGF401)[e]	FGFR4	118036971	$C_{25}H_{30}N_8O_4$	2/9	507	0.6	Unkn	Only 1 clinical trial targeting solid tumors with FGFR4 expression (NCT02325739).
(H3B-6527)[e]	FGFR4	118029202	$C_{29}H_{34}Cl_2N_8O_4$	3/9	630	4.4	Unkn	Only 2 clinical trials with one targeting HCC.
Inhibitors without drug-FGFR X-ray crystal structures								
Nintedanib (BIBF-1120) Vargatef	FGFR1, VEGFR2/3, PDGFRα	135423438	$C_{31}H_{33}N_5O_4$	2/7	540	4.3	No	Idiopathic pulmonary fibrosis (2014). A total of 152 trials with one targeting FGFR3 dysregulated urothelial cancers. Other targets include RCC, pancreatic, breast, thyroid, cervical, endometrial, lung, ovarian, and prostate cancers and HCC and NSCLC.
Pazopanib (GW786034) Votrient	FGFR1, VEGFR1/2/3, PDGFRβ, Kit	10113978	$C_{21}H_{23}N_7O_2S$	2/8	438	3.1	No	RCC and soft tissue sarcomas (2009). A total of 304 trials including one targeting FGFR2 amplification in solid tumors (NCT02450136). Others are targeting sarcomas, melanomas and RCC, breast, ovarian, bladder, stomach, and prostate cancers, NSCLC, GIST, and glioblastomas.
Pemigatinib (INCB054828)	FGFR1/2/3/4	86705695	$C_{24}H_{27}F_2N_5O_4$	1/8	488	1.8	Unkn	A total of 13 clinical trials targeting myeloid neoplasms, urinary bladder cancers, advanced solid tumors, cholangiocarcinomas, and AML. Five trials are targeting FGFR alterations.
Rogaratinib (BAY 1,163,877)	FGFR1/2/3/4	71611869	$C_{23}H_{26}N_6O_3S$	2/8	467	1.7	Yes	A total of 8 clinical trials targeting urinary bladder cancer, NSCLC, and other solid tumors. Three trials are targeting FGFR alterations.
Fisogatinib (BLU-554)[e]	FGFR4	91885617	$C_{24}H_{24}Cl_2N_4O_4$	2/7	503	4.7	No	A single clinical trial targeting hepatocellular carcinomas (NCT02508467).
(PRN1371)[e]	FGFR1/2/3/4, CSF1R	118295624	$C_{26}H_{30}Cl_2N_6O_4$	1/8	562	3.5	Unkn	A single clinical trial targeting bladder cancer (NCT02608125).

[a] www.ncbi.nlm.nih.gov/pccompound.
[b] No. of hydrogen bond donors/acceptors.
[c] Produces hyperphosphatemia; Unkn, unknown.
[d] ALL; acute lymphoblastic leukemias; AML, acute myeloid leukemias; CML, chronic myelogenous leukemias; GIST, gastrointestinal stromal tumors; HCC, hepatocellular carcinomas, NSCLC, non-small cell lung cancers, RCC, renal cell cancers.
[e] Type VI covalent inhibitor.

Table 9
Specificities of FGFR protein-tyrosine kinase inhibitors with IC_{50} values in nM.

Agent	FGFR1	FGFR2	FGFR3	FGFR4	VEGFR2
FGFR1/2/3 inhibitors					
AZD4547	0.2	1.8	2.5	165	24
Debio1347	9.3	7.6	22	290	2100
Infigratinib	0.9	1.4	1.0	60	180
Pemigatinib	0.4	0.5	1.2	30	?
FGFR4 inhibitors					
Roblitinib[a]	$> 10^4$	$> 10^4$	$> 10^4$	2	$> 10^4$
H3B-6527[a]	320	1290	1060	1.2	?
Fisogatinib[a]	506	801	1540	4	?
Pan-FGFR inhibitors					
Erdafitinib	2.0	2.0	4.0	6.3	50
Futibatinib[a]	3.9	1.3	1.6	8.3	?
LY2874455	2.8	2.6	6.4	6.0	5
Rogaratinib	12	1	19	33	120
PRN1371[a]	0.6	1.3	4.1	19.2	?
Multi-kinase inhibitors					
Dovitinib	10	400	3.2	4000	20
Lenvatinib	22	8.2	15	14	0.74
Lucitanib	7	?	?	?	2.4
Nintedanib	38	?	?	?	5
Pazopanib	84	?	?	?	30
Ponatinib	2.2	1.6	18.2	7.7	1.5

[a] Covalent inhibitor.

erdafitinib, AZD4547 produces hyperphosphatemia [82].

Sohl et al. determined the X-ray crystal structure of AZD4547 bound to the activated gatekeeper mutant of *FGFR1* (V561 M) [81]. The AZD4547 hydrogen bonds with E562 and A564 as seen in the wildtype enzyme, but there is no hydrogen bond with DFG-D641 as the flexible ethyl group in the therapeutic allows for the translocation of the 3,5-dimethoxyphenyl group (Fig. 9E). The hydrophobic interactions of AZD4547 with the mutant enzyme are nearly the same as those described above with the exception of a lack of interaction with RS2, RS3, F489 of the glycine-rich loop and E531 and M535 of the αC-helix. In contrast to its binding to the wildtype enzyme, AZD4547 fails to bind to the gate area or back pocket of the mutant and it does not extend past the gatekeeper residue; instead, it interacts with the front pocket and FP-II. The mutant drug-enzyme complex corresponds to that of a type I½B inhibitor (inactive DFG-D_{in} conformation with the autoinhibitory brake and a closed activation segment) [60]. Fig. 9F shows the superposition of the drug binding to the wildtype and gatekeeper mutants.

5.5. CH5183284/Debio 1347

This drug is an indole-aminopyrazole derivative (Fig. 8E) that specifically inhibits FGFR1/2/3 with IC_{50} values of 9.3/7.6/22 nM and that for FGFR4 of 290 nM and the pharmaceutical is classified as a FGFR1/2/3 inhibitor (Table 9) [75,83,84]. Its IC_{50} values vs. VEGFR1/2, Kit, Flt3, and PDGFRβ are 2–3 orders of magnitude greater [75]. It is in three clinical trials in patients with breast cancer and other solid tumors (Table 8). Nakanishi et al. determined the X-ray crystal structure of CH5183284 bound to FGFR1 [83]. The amino group of the compound forms a hydrogen bond with the carbonyl oxygen of E562 (the first hinge residue), the ketone oxygen forms a hydrogen bond with the N−H group of A564, and the indole N−H group forms a hydrogen bond with the carbonyl group of A564 (Fig. 9G). The pharmaceutical makes apolar contact with five spine residues (RS2/3, CS6/7/8), two shell residues (Sh1/2), and the KLIFS-3 residue. It also makes hydrophobic contact with AVK514, Y563, A564, and S565 of the hinge, A640 (the x of xDFG), and DFG-D641. Nakanishi et al. report that the interactions of (i) the benzimidazole methyl group with F642, (ii) the benzimidazole nitrogen with the sulfur atom of M535, and (iii) the benzimidazole aromatic ring with the gatekeeper (M561) play an important role in promoting the interaction specificity of CH5183284 with FGFR1/2/3 [83]. The compound occupies the front cleft, gate area, and BP-I-B while not extending past the gatekeeper and it binds to a DFG-D_{in} inactive enzyme (with the autoinhibitory brake and a closed activation segment). The drug is classified as a Type I½B inhibitor [60]. It is unknown whether CH5183284 produces hyperphosphatemia.

5.6. Infigratinib

The pharmaceutical is a pyrimidine derivative (Fig. 8F) that inhibits FGFR1/2/3 with IC_{50} values of 0.9/1.4/1.0 nM and FGFR4 with an IC_{50} value of 60 nM [75,85]. Accordingly, infigratinib is classified as a FGFR1/2/3 inhibitor (Table 9). Its IC_{50} for VEGFR2 is 180 nM; its effectiveness against other protein kinases has not been examined. The therapeutic is in 16 clinical trials, six of which are directed at patients with FGFR dysregulation (Table 8). Guagnano et al. determined the X-ray crystal structure of infigratinib bound to FGFR1 [85]. It shows that the pyrimidine *N*3 forms a hydrogen bond with the N−H group of A564 (the third hinge residue) and the amino group of the ligand forms a hydrogen bond with the carbonyl group of A564 (Fig. 9H). Moreover, one of the methoxy oxygens forms a polar bond with the N−H group of DFG-D641 and the piperazine *N*4 N−H group hydrogen bonds with the carboxylate side chain of E571 within the αD-helix. Infigratinib makes hydrophobic contact with five spine residues (RS2/3 and CS6/7/8), all three shell residues (Sh1/2/3), and KLIFS-3. The agent also interacts hydrophobically with V513 and K514 of the β3-strand, E531 and M535 of the αC-helix, E562, Y563, and A564 of the hinge, A640 (the x of xDFG), and with DFG-D641. The pharmaceutical occupies the front cleft, gate area, back cleft, BP-I-A, and BP-I-B (Table 10). Infigratinib binds to an inactive structure with the autoinhibitory brake, a closed activation segment, and the DFG-D_{in} conformation; the drug extends past the gatekeeper residue and it is classified as a Type I½A inhibitor [60]. Like erdafitinib, infigratinib produces hyperphosphatemia in patients [86].

5.7. Lenvatinib

Lenvatinib is a quinoline derivative (Fig. 8G) that blocks the activity of several protein kinases [87,88]. Its IC_{50} values for FGFR1/2/3/4 are 22/8.2/15/14 nM, for VEGFR1/2/3 are 1.3/0.74/0.71 nM, for RET is 1.5 nM, and for Kit is 11 nM [88]. Based upon these data, lenvatinib is classified as a multi-kinase antagonist (Table 9). The therapeutic was FDA approved for the treatment of differentiated thyroid cancer in 2015 and is currently in more than 100 clinical trials (Table 8) several of which include patients with diseases associated with FGFR dysfunction. Matsuki et al. determined the structure of this pharmaceutical bound to FGFR1 [89]. The results demonstrate that *N*1 of the quinoline group forms a hydrogen bond with the A564 N−H group of the third hinge residue, the two ureido N−H groups interact with the carboxylate side chain of αC-E531, and the ureido oxygen forms a hydrogen bond with the DFG-D641 N−H group (Fig. 9I). Lenvatinib makes hydrophobic contact with five spine residues (RS2/3 and CS6/7/8), two shell residues (Sh1/2), and KLIFS-3 (Table 10). The pharmaceutical also interacts hydrophobically with F489 within the glycine-rich loop (the Φ of GxGxΦG), the β3-AVK514, E531 and M535 of the αC-helix, E562, Y563, A564, and S565 of the hinge, and A640 (the x of xDFG). The ligand occupies the front cleft, gate area, back cleft, BP-I-A, BP-I-B, and BP-II-in and it extends past the gatekeeper residue. Lenvatinib binds to an inactive enzyme with the autoinhibitory brake, a closed activation segment, and the DFG-D_{in} conformation; it is classified as a Type I½A inhibitor [60]. Lenvatinib has not been shown to increase serum phosphate levels.

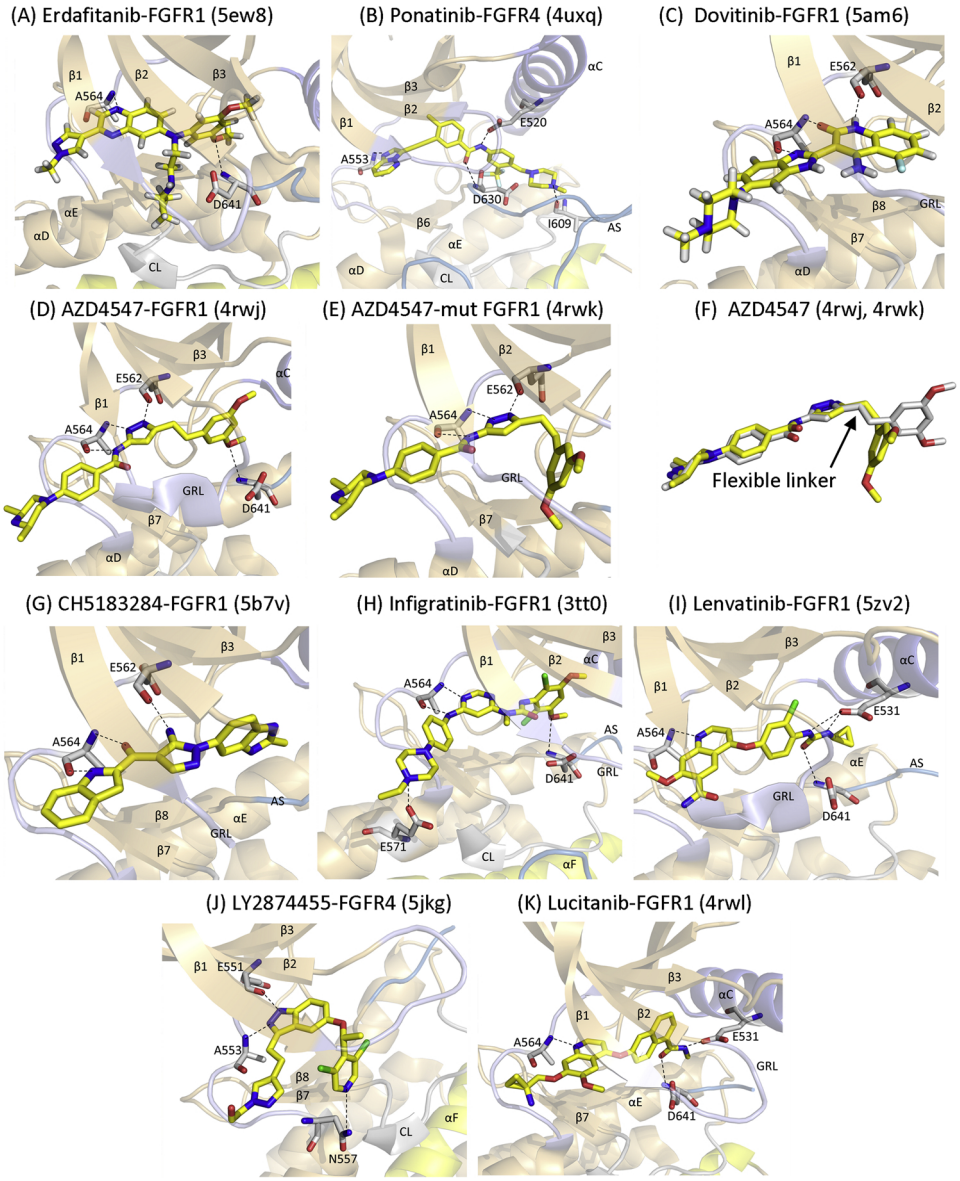

Fig. 9. Structures of reversible drug-FGFR complexes. The PDB IDs are given in the parentheses.

Table 10
Human drug-enzyme hydrophobic (Φ) interactions using their designated KLIFS residue numbers[a].

	PDB ID	RS1	RS2	RS3	Sh1	Sh2	Sh3	CS6	CS7	CS8	KLIFS-3	KLIFS pockets[b] & subpockets
KLIFS no. →		68	82	28	36	45	43	77	11	15	3	
Drug-enzyme ↓												
Erdafitinib-FGFR1	5ew8		Φ	Φ	Φ	Φ	Φ	Φ	Φ	Φ	Φ	F, G, B, FP-I, BP-I-A/B
Ponatinib-FGFR4	4uxq, 4tyj, 4qrc	Φ	Φ	Φ	Φ	Φ	Φ	Φ	Φ	Φ	Φ	F, G, B, BP-I-A/B, BP-II-out, BP-III/IV
Dovitinib-FGFR1	5am6				Φ	Φ		Φ	Φ	Φ	Φ	F
Dovitinib-mutant FGFR1	5am7				Φ	Φ		Φ	Φ	Φ	Φ	F
AZD4547-FGFR1	4rwj		Φ	Φ	Φ	Φ	Φ	Φ	Φ	Φ	Φ	F, G, B, BP-I-A/B
AZD4547-mutant FGFR1	4rwk				Φ	Φ		Φ	Φ	Φ	Φ	F, FP-II
CH5183284-FGFR1	5b7v		Φ	Φ	Φ	Φ		Φ	Φ	Φ	Φ	F, G, BP-I-B
Infigratinib-FGFR1	3tt0		Φ	Φ	Φ	Φ	Φ	Φ	Φ	Φ	Φ	F, G, B, BP-I-A/B
Lenvatinib-FGFR1	5zv2		Φ	Φ	Φ	Φ		Φ	Φ	Φ	Φ	F, G, B, BP-I-A/B, BP-II-in
LY2874455-FGFR4	5jkg				Φ	Φ		Φ	Φ	Φ	Φ	F
Lucitanib-FGFR1	4rwl		Φ	Φ	Φ	Φ	Φ	Φ	Φ	Φ	Φ	F, G, B, BP-I-A/B, BP-II-in
Futibatinib-FGFR1	6mzw		Φ	Φ	Φ	Φ	Φ	Φ	Φ	Φ	Φ	F, G, B, BP-I-A/B
Roblitinib-FGFR4	6jpj				Φ	Φ		Φ	Φ	Φ	Φ	F
H3B-6527-FGFR4	5vnd		Φ	Φ	Φ	Φ	Φ	Φ	Φ	Φ	Φ	F, G, B, BP-I-A/B

[a] KLIFS-3, kinase-ligand interaction fingerprint and structure residue-3; from http://klifs.vu-compmedchem.nl/.
[b] F, front pocket; G, gate area; B, back pocket.

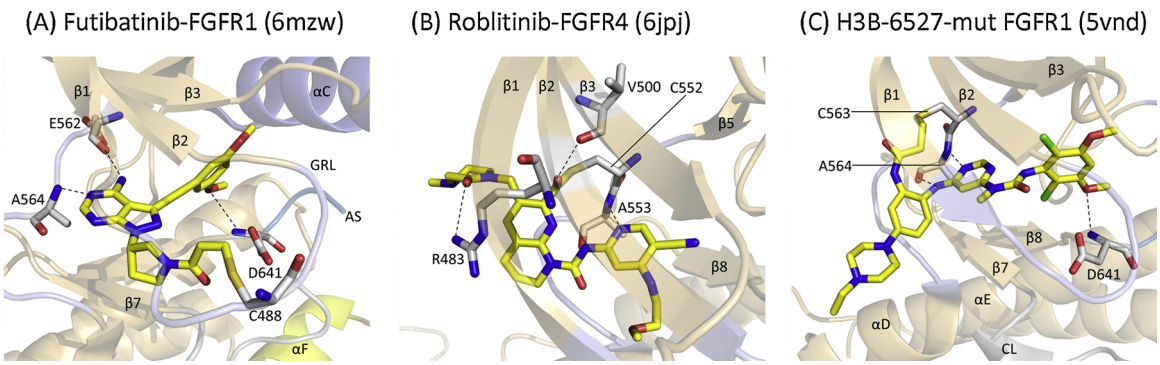

Fig. 10. Structures of covalent drug-FGFR complexes. The PDB IDs are given in parentheses.

5.8. LY2874455

LY2874455 is a pyrazole-indazole derivative (Fig. 8H) that inhibits FGFR1/2/3/4 with IC_{50} values of 2.8/2.6/6.4/5 nM and the pharmaceutical is classified as a pan-FGFR blocker (Table 9) [90]. It is 6–9 fold more potent in blocking FGF signaling that VEGF signaling in vivo. The therapeutic is in two clinical trials, one of which is based upon potential FGFR dysfunction (Clinical trials identifier: NCT01212107). Wu et al. determined the X-ray crystal structure of the pharmaceutical bound to FGFR4 [91]. This shows that the *N*1 indazole N−H hydrogen bonds with the backbone carbonyl group of E551 and the *N*2 nitrogen hydrogen bonds with the N−H group of A553 (the third hinge residue); the pyridine nitrogen hydrogen bonds with the side chain N−H group of N557 at the end of the hinge region (Fig. 9J). The pharmaceutical makes hydrophobic contact with three spine residues (CS6/7/8), two shell residues (Sh2/3), and KLIFS-3. It also makes hydrophobic contact with E465 within the glycine-rich loop, the β3 AVK503, C552, A553, A554, K555, and N557 within the hinge region, R616 within the catalytic loop, and A629 (the x of xDFG). The compound occupies the front cleft only. The activation segment is disordered and one cannot tell whether it is in an open or closed configuration. However, the enzyme exhibits an autoinhibitory brake and is thus inactive. Based upon these observations, LY2874455 is classified as a type I½B inhibitor of FGFR4 [60]. Furthermore, this pharmaceutical produces hyperphosphatemia [92].

5.9. Lucitanib

Lucitanib is a quinoline derivative bearing aminocyclopropyl and naphthalene substituents (Fig. 8I) that was initially developed as an angiogenesis inhibitor [93]. Its IC_{50} values for FGFR1 (7 nM), VEGFR1/2 (12/4 nM), Src (4.9 nM), and PDGFRα/β (13/8 nM) are in the low nM range and the drug is classified as a multi-kinase inhibitor (Table 9); its IC_{50} values for RET, Kit, and Src are orders of magnitude higher. Sohl et al. determined the X-ray crystal structure of the pharmaceutical bound to FGFR1 [81]. It demonstrates that the *N*1 of the quinoline scaffold makes a hydrogen bond with the N−H group of A564 (the third hinge residue), the carboxamide oxygen hydrogen bonds with the N−H group of DFG-D641, and the amide group forms a hydrogen bond with αC-E531 (Fig. 9K). The pharmaceutical makes hydrophobic contact with five spine residues (RS2/3, CS6/7/8), three shell residues (Sh1/2/3), and the KLIFS-3 valine residue (Table 10). Lucitanib also interacts hydrophobically with the β3-strand AVK514, E531 of the αC-helix, E562, Y563, A564, S565 of the hinge region, A640 (the x of xDFG), and L644 within the activation segment. The agent occupies the front cleft, gate area, back cleft, BP-I-A, BP-I-B, and BP-II-in (Table 10). The compound is bound to a DFG-D_{in} inactive conformation of FGFR1 with the autoinhibitory brake and a closed activation segment. Overall this interaction corresponds to that of a type I½A inhibitor [60]. Unlike erdafitinib, lucitanib does not produce hyperphosphatemia [67]

6. Structures of covalent drug-FGFR complexes and common drug-enzyme interactions

6.1. Futibatinib

This pharmaceutical is a pyrazolo[3,4-*d*]pyrimidine derivative (Fig. 8J) that inhibits FGFR1/2/3/4 with IC_{50} values of 3.9/1.3/1.6/8.3 nM and futibatinib is classified as a pan-FGFR antagonist (Table 9) [94]. Its inhibitory activity against other protein kinases has not been tested. The pharmaceutical is in four clinical trials, two of which are in patients with FGFR2 dysregulation (Table 8). Kalyukina et al. determined the X-ray crystal structure of this agent covalently bound to FGFR1 [94]. It shows that the 4-amino group of the pyrimidine forms a hydrogen bond with the carbonyl group of E562 and *N*3 forms a hydrogen bond with the N−H group of A564 (the third hinge residue, Fig. 9H). The oxygen atom of one of the methoxy groups forms a hydrogen bond with the backbone N−H group of DFG-D641 while the compound forms a covalent Michael adduct with C488 (Fig. 10A). Futibatinib makes hydrophobic contact with five spine residues (RS2/3 and CS6/7/8), all three shell residues (Sh1/2/3), and KLIFS-3 (Table 10). The medicinal also makes hydrophobic contact with F489 of the glycine-rich loop, V492 within the β2-strand, AVK514 of the β3-strand, E531 and M535 of the αC-helix, Y563 within the hinge, A640 (the x of xDFG), and DFG-D641. The compound occupies the front cleft, gate area, back cleft and BP-I-A and BP-I-B. The drug is classified as a type VI covalent inhibitor. Owing to the disorder of the activation segment, one cannot classify it as open or closed. However, the enzyme exhibits the autoinhibitory FGFR brake (not shown) and is therefore in an inactive conformation. Like erdafitinib, futibatinib produces hyperphosphatemia [95].

6.2. Roblitinib

The pharmaceutical is a 1,8-naphthyridine pyridine derivative (Fig. 8K) with an IC_{50} value of 2 nM against FGFR4 [96]. It fails to inhibit FGFR1/2/3, VEGFR2, and RET with IC $_{50}$ values greater than 10 μM; roblitinib is classified as a FGFR4 blocker (Table 9). The therapeutic has been in a clinical trial against hepatocellular carcinomas expressing FGFR4 (NCT02325739). Zhou et al. determined the structure of this pharmaceutical covalently bound to FGFR4 [97]. The aldehyde moiety of the compound forms a hemithioacetal with C552 and the resulting hydroxyl group hydrogen bonds with V500 within the β3-strand (Fig. 10B). Moreover, the pyridine nitrogen forms a hydrogen bond with the N−H group of A553 (the third hinge residue), and the oxygen from the piperazinyl group forms a hydrogen bond with guanidinium group of R483 within the β2-strand. Roblitinib makes hydrophobic contact with three spine residues (CS6/7/8), two shell residues (Sh1/2), and KLIFS-3. It also makes hydrophobic contact with AVK503 of the β3-strand and E551, C552, A553, and A554 within the hinge. The pharmaceutical occupies the front pocket and does not

extend past the gatekeeper residue. Roblitinib binds to an inactive (autoinhibited brake, closed activation segment) DFG-D_{in} enzyme form; the ligand binds covalently to FGFR4 and is classified as a Type VI inhibitor [60]. It is unknown whether roblitinib produces hyperphosphatemia.

6.3. H3B-6527

The pharmaceutical is a pyrimidine derivative (Fig. 8L) and a potent inhibitor of FGFR4 (IC_{50} < 1.2 nM) with little activity against FGFR1/2/3 (320/1290/1060 nM) or CSF1R (> 10 μM) [98]. Accordingly, H3B-6527 is classified as a FGFR4 antagonist (Table 9). The agent is in two clinical trials with one targeting HCC (NCT02834748). Joshi et al. determined the X-ray crystal structure of the drug covalently bound to a *FGFR1* Y563C mutant that serves as a surrogate for FGFR4 [98]. Residue 563 corresponds to the second hinge residue and is a cysteine in FGFR4, but it is a tyrosine in FGFR1/2/3. This genetic alteration in FGFR1 essentially mirrors the ATP-binding pocket in FGFR4. The structure demonstrates that the pyrimidine nitrogen hydrogen bonds with the N—H group of A564 and the amino group of the pharmaceutical hydrogen bonds with the carbonyl group of A564 (the third hinge residue). Moreover, an oxygen of one of the methoxy groups hydrogen bonds with the N—H group of DFG-D641 and the acrylamide group forms a covalent linkage with C563 (Fig. 10C). The compound makes hydrophobic contact with five spine residues (RS2/3 and CS6/7/8), three shell residues (Sh1/2/3), and KLIFS-3. It also makes hydrophobic contact with L494, V511, V513, and K514 of the β3-strand, E531 and M535 of the αC-helix, V559 of the β5-strand, E562 and A564 of the hinge, and E571 of the αD-strand. The drug occupies the front pocket, gate area, back pocket, BP-I-A and BP-I-B. The enzyme exhibits an inactive conformation with the autoinhibitory brake and a closed activation segment. It is classified as a Type VI inhibitor owing to its covalent attachment to the target enzyme [60]. It is unknown whether H3B-6527 produces hyperphosphatemia.

6.4. Shared interactions of the above drugs with the fibroblast growth factor receptors

Each of the above pharmaceuticals makes hydrophobic contact with catalytic spine residues CS5/6/7 and shell residues Sh1/2 (Table 10). All of the drugs form one or two hydrogen bonds with the third hinge residue (KLIFS 48). Moreover, each of the pharmaceuticals makes hydrophobic contact with KLIFS residues 3 and 17 (Fig. 11). All of the drugs also make hydrophobic contact with KLIFS-47 (the second hinge residue). CS7 (alanine), CS8 (valine), KLIFS-3 (valine), and KLIFS-17 (lysine) are conserved residues throughout the protein-tyrosine kinase family. Besides the third hinge residue, dovitinib, AZD4547, CH5183214, futibatinib, and LY2874455 also form hydrogen bonds with the first hinge residue. Furthermore, erdafitinib, AZD4547, CH5183214, infigratinib, lenvatinib, lucitanib, futibatinib, ponatinib, and LY2874455 interact hydrophobically with the residue immediately before the activation segment (xDFG, or KLIFS-80). AZD4547, infigratinib, lenvatinib, futibatinib, and H3B-6527 interact hydrophobically with a glutamate (KLIFS-24) and methionine (KLIFS-28) within the αC-helix; these pharmaceuticals occupy subpockets BP-I-A and BP-I-B. The pockets and subpockets with which these drugs interact with are listed in Table 10 and their locations are illustrated in Fig. 7. The formation of a hydrogen bond with the third hinge residue and hydrophobic interactions with CS6/7/8, Sh1/2, and KLIFS residue-3 is a property that the aforementioned pharmaceuticals share with all of the FDA-approved protein kinase inhibitors that interact directly with the kinase domain [43].

7. Inhibitors lacking drug-FGFR X-ray crystal structures

Nintedanib is an indole carboxylate derivative (Fig. 8M) that is an

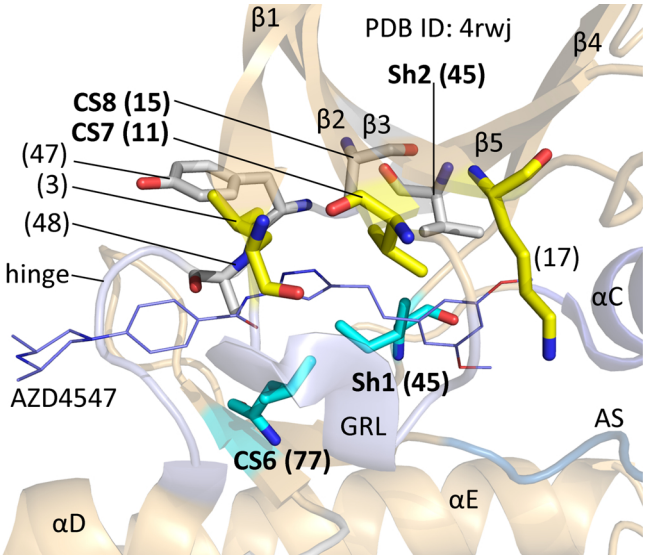

Fig. 11. Shared interactions of drugs with fibroblast growth factor receptors. The amino acid residues that are colored yellow are on this side of the drug, the gray residues are on the other side of the drug, and the cyan residues are below the drug (AZD4547). The KLIFS residue numbers [42] are in parentheses. Prepared from PDB ID: 4rwj.

inhibitor of (i) FGFR1 with an IC_{50} value of 38 nM, (ii) VEGFR1/2/3 with values of 104/5/5, and (iii) PDGFRα with a value of 18 nM [99]. Accordingly, nintedanib is classified as a multi-kinase inhibitor (Table 9). It was initially developed as a VEGFR inhibitor for the treatment of a variety of solid tumors. The therapeutic was FDA-approved (2014) for the treatment of idiopathic pulmonary fibrosis, which may be due to its inhibition of FGFR1/2/3. It is undergoing clinical trials targeting a variety of cancers as indicated in Table 8. We lack X-ray crystal structures of the compound bound to any of the FGFRs, but Terzyan et al. determined its mode of binding to the RET protein-tyrosine kinase [100]. They found that the N—H group of the indole forms a hydrogen bond with the first hinge residue and the 2-carbonyl oxygen forms a hydrogen bond with the N—H group of the third hinge residue (PDB ID: 6nec). The carbonyl moiety attached to the indole group forms a hydrogen bond with the RET DFG-D aspartate. The pharmaceutical binds to an active conformation of RET and is thus a Type I inhibitor. Whether nintedanib binds to FGFR1/2/3 in a similar fashion remains to be established. The therapeutic is not known to produce hyperphosphatemia.

Pazopanib is an indazolylpyrimidine derivative (Fig. 8N) that is an inhibitor of VEGFR1/2/3 with IC_{50} values of 10/30/47 nM; moreover, it inhibits PDGFRβ, Kit, and FGFR1 with IC_{50} values of 84, 74, and 140 nM, respectively [101]. The pharmaceutical is classified as a multi-kinase inhibitor (Table 9). Although these inhibitory values are not impressive, pazopanib is FDA-approved for the treatment of renal cell carcinomas and soft tissue sarcomas (www.brimr.org/PKI/PKIs.htm). The therapeutic is in or has been in more than 200 clinical trials targeting a variety of tumor types (Table 8). We lack crystal structures of the compound bound to any protein kinase. It has two hydrogen bond donors and eight hydrogen bond acceptors suggesting a large number of possible binding modes to its target enzymes. Harris et al. determined the X-ray crystal structure of a pazopanib congener with VEGFR2 and found that the pyrimidine and adjacent amino group form hydrogen bonds with the third hinge residue [101]. Whether this mirrors the binding of pazopanib to any of the FGFRs remains to be determined. Early studies identify pazopanib as a promising treatment for pediatric soft tissue sarcomas [102]. The pharmaceutical is not known to produce hyperphosphatemia.

Pemigatinib is a tetra-azatricyclotridecatetraene derivative

(Fig. 8O) that is a potent inhibitor of FGFR1/2/3 [103]. Its IC_{50} values for FGFR1/2/3/4 are 0.4/0.5/1.2/30 nM, respectively. Accordingly, the drug is classified as a FGFR1/2/3 blocker (Table 9). Its effectiveness in inhibiting other protein kinases has not been reported. It is in five clinical trials against tumors possessing FGFR alterations (ClinicalTrials.gov). Information on the nature of its binding to target enzymes is lacking and it is unknown whether the therapeutic produces hyperphosphatemia.

Rogaratinib is a pyrrolotriazine derivative (Fig. 8P) that was designed as a specific inhibitor of the FGFRs [104]. It is a potent inhibitor of FGFR1/2/3/4 with IC_{50} values of 12/ < 1/19/33 nM and the pharmaceutical is classified as a pan-FGFR blocker. Rogaratinib has not been tested against a large panel of protein kinases, but it is a less potent inhibitor of VEGFR2 (IC_{50} of 120 nM) which would minimize some of its potential side effects. It is in clinical trials against a variety of solid tumors as listed in Table 8. The compound possesses two hydrogen bond donors and eight hydrogen bond acceptors and there are many possible ways that this drug could interact with the its target enzymes. However, there is no structural information on its mode of binding with its targets. Like erdafitinib, rogaratinib produces hyperphosphatemia [105].

Fisogatinib is a quinazoline derivative bearing an acrylamide group (Fig. 8Q) that targets FGFR4 with an IC_{50} value of 4 nM while the values for FGFR1/2/3 are 506/801/1540 nM and this medicinal is classified as a FGFR4 antagonist (Table 9) [106]. FGFR4 bears a cysteine at position 552 (the second hinge residue) that reacts with the acrylamide group to form a Michael adduct whereas FGFR1/2/3 lack a comparable cysteine at this location. The therapeutic is in a clinical trial targeting patients with hepatocellular carcinomas. Owing to the covalent nature of its binding to FGFR4, the pharmaceutical is classified as a Type VI inhibitor [60]. Afatinib and dacomitinib are FDA-approved Type VI covalent protein kinase inhibitors that possess, like fisogatinib, a quinazoline scaffold. Afatinib and dacomitinib are inhibitors of the epidermal growth factor receptor family that are used in the treatment of NSCLC [43]. Fisogatinib does not produce hyperphosphatemia [69]. See Ref. [71] for a summary of clinical trials involving FGFR therapeutics.

PRN1371 is a pyrido[2,3-*d*]pyrimidine derivative bearing an enoylpiperazine group (Fig. 8R) that inhibits FGFR1/2/3/4 and CSF1R with IC50 values of 0.6/1.3/4.1/19.3, and 8.1 nM, but fails to inhibit a panel of some 250 other protein kinases [107]. Accordingly, PRN1371 is classified as a pan-FGFR blocker (Table 9). The compound was designed to covalently bond to FGFR1 C488, which occurs within the glycine-rich loop. A comparable residue occurs in FGFR2/3/4 and only three other protein kinases. Moreover, a comparable cysteine is lacking in closely related off-targets such as VEGFR1/2/3 and PDGFRα/β. The therapeutic is in a phase I clinical trial in patients with metastatic urothelial carcinomas. Owing to the covalent nature of its binding to FGFR1/2/3/4, PRN1371 is classified as a Type VI inhibitor [60]. It is not known whether PRN1371 produces hyperphosphatemia.

8. Epilogue and perspective

The Kit signaling family includes only the stem cell factor (SCF) and its Kit receptor while the PDGFR family involves four growth factors and two receptors (Table 11). The VEGFR family includes five growth factors and three receptors while the ErbB family consists of 11 growth factors and four receptors. The FGF family is one of the largest, if not the largest, signaling constellation with a total of 22 growth factors, four protein-kinase receptors, and a fifth receptor lacking intracellular enzyme activity. The potential combinations of FGF1–23 and FGFR1–4 interactions numbers in the thousands. This multiplicity increases the difficulty in deciphering specific signaling pathways. The FGFR family plays an integral role in human development [3]. Moreover, there is a considerable interplay of factors produced in mesenchymal tissue with receptors expressed in epithelial cells. Similarly, there is extensive interaction between FGFs and their receptors in tumor cells and tumor stromal cells.

Although this review focuses on the role of fibroblast growth factor receptor dysregulation during neoplastic transformation, there are dozens of skeletal diseases related to *FGFR* genetic abnormalities [3]. One of the more common of these disorders is achondroplasia, a form of short-limbed dwarfism. The pathogenesis of achondroplasia results from an inability to convert cartilage to bone during ossification, particularly in the long bones of the arms and legs. People with achondroplasia have short stature. The average height of an adult male with achondroplasia is 4 feet, 4 in. (131 cm) and the average height of an adult female is 4 feet, 1 inch (124 cm). An autosomal dominant G380R mutation in the *FGFR3* gene is the predominant cause of achondroplasia [109]. This mutation within the transmembrane segment causes the FGFR3 protein to exhibit increased activity, which interferes with skeletal development and leads to the disturbances in bone growth seen with this disorder.

Additional skeletal anomalies with *FGFR3* mutations were subsequently detected in thanatophoric dysplasia, hypochondroplasias, and other maladies whose clinical phenotypes resemble achondroplasia [3]. Thanatophoric dysplasia is the most common lethal form of dwarfism. Besides the shortened limbs, an underdeveloped thoracic cavity leads to respiratory insufficiency and death at birth or soon thereafter. The type I dysplasia is due to a K650E mutation within the activation segment and the type II dysplasia is commonly due to an R248C mutation that is found between the extracellular D2 and D3 domains [110]. Pfeiffer syndrome results from mutations of either *FGFR1* or *FGFR2* [111]. This syndrome is a rare genetically heterogeneous autosomal dominant disorder that is characterized by the premature fusion of certain bones of the skull (craniosynostosis) and affects the shape of the head and face. FGFRL1 is a fibroblast growth factor receptor-like protein with a large extracellular FGF-binding component and short 105-residue intracellular portion. Its function is unknown, but a frameshift insertion encoding residues near its carboxyterminus causes an elongation of the FGFRL1 polypeptide chain from 504 amino acid residues to 551 residues resulting in craniosynostosis. This suggests that this receptor may also play a part in skeletal development. See Ref [3]. for a list of the large number of musculoskeletal disorders related to *FGF* and *FGFR* mutations.

A major problem with all protein kinase antagonists involves the development of resistance to these therapeutics [112]. Clinical data on the molecular mechanisms of resistance to FGFR therapeutics are limited owing to the recent development and use of these compounds. However, Goyal et al. analyzed longitudinal blood samples for circulating tumor DNA (ctDNA) and cholangiocarcinoma tumor samples in patients receiving infigratinib during the progression of neoplasms bearing three different *FGFR2* translocations (*FGFR2-ZMYM4, FGFR2-OPTN, FGFR2-BICC1*) [113]. DNA sequencing revealed the occurrence of several resistance mutations in the FGFR2 protein kinase domain including N549 H/K, V564 F (the gatekeeper), E565A, L617 V, K641R and K659 M. The first patient possessed N549 H/K, V564 F, E565A, and K659 M mutations, the second patient possessed N549H, V564 F, L617 V, and K641R mutations, and the third patient possessed a single V564 F mutation. Note that the gatekeeper mutation was observed in all three patient samples [113], and gatekeeper mutations are one of the most common causes of acquired resistance involving numerous protein kinases [114]. Whether these and other resistance mutations occur in response to the treatment of other neoplasms with different FGFR antagonists remains to be established. Moreover, additional *FGFR* resistance mutations, activation of by-pass pathways, and mutations in other gene products such as *PTEN* or *PIK3CA* are anticipated as other drugs such as erdafitinib and different tumors including urothelial urinary bladder cancers are examined during extended periods of treatment.

Cisplatin-based combination therapies with (i) M-VAC (methotrexate, vinblastine, doxorubicin (Adriamycin) and cisplatin), (ii)

Table 11
Growth factor families.

Growth factor receptors [reference]	Growth factors
Kit [34]	Stem cell factor (SCF)
PDGFRα/β [108]	PDGF-A/B/C/D
VEGFR1/2/3 [39]	VEGF-A/B/C/D, placental growth factor (PlGF)
ErbB1/2/3/4 [29,30] [a]	EGF, epigen (EPG), transforming growth factor-α (TGF-α), amphiregulin (AR), betacellulin (BTC), heparin-binding epidermal growth-factor like growth factor (HB-EGF), epiregulin (EPR), neuregulin-1/2/3/4 (Nrg-1/2/3/4)
FGFR1-IIIB & IIIC/FGFR2-IIIB & IIIC/FGFR3-IIIB & IIIC/FGFR4/FGFRL1	22 FGF gene products

[a] Members of the epidermal growth factor receptor (EGFR) family.

cisplatin, methotrexate and vinblastine (CMV), or (iii) gemcitabine, cisplatin, and paclitaxel (GCP) are the standard care for patients with metastatic bladder cancer [115]. One of the theoretical advantages of using these combination-based cisplatin therapies is to lessen the occurrence of drug resistance [116]. Moreover, atezolizumab, durvalumab, and avelumab are anti-PD-L1 antibodies that are approved for second-line treatment of patients with advanced bladder cancers following platinum-based chemotherapy. Similarly, pembrolizumab and nivolumab are anti-PD-1 antibodies that are approved for the second-line treatment of bladder cancers. These five monoclonal antibodies function as immune checkpoint inhibitors. Erdafitinib is a pan-FGFR inhibitor that is approved for the second-line treatment of bladder cancers following platinum-based therapy. Although reliant on only early findings, Loriot et al. surmised that responses to erdafitinib in bladder cancers may be more robust than their response to immune checkpoint inhibitors [66]. Additional studies will be required to substantiate or refute this hypothesis. The next-generation sequencing data argue for the potential efficacy of targeting FGFRs in a wide variety of other cancers that harbor *FGFR* alterations [48]. There are no protein kinase antagonists approved for the treatment of prostate cancers. Based upon the association of *FGFR1/2/4* gene alterations (*FGFR1* amplification, *FGFR2-PPAPDC1A* translocation, *FGFR4* amplification, and a *FGFR4 R610H* mutation) with prostate cancer [48], this common malignancy represents a potential disease that might respond to FGFR inhibitors. The development of FGFR antagonists has lagged behind those of other receptor protein-tyrosine kinases [117]. However, the approval of erdafitinib may stimulate additional work targeting the many other FGFR-driven neoplasms, including those of prostate cancer.

Declaration of Competing Interest

The author is unaware of any affiliations, memberships, or financial holdings that might be perceived as affecting the objectivity of this review.

Acknowledgments

The author thanks Laura M. Roskoski for providing editorial and bibliographic assistance. I also thank Jasper Martinsek and Josie Rudnicki for their help in preparing the figures and W.S. Sheppard and Pasha Brezina for their help in structural analyses. The colored figures in this paper were evaluated to ensure that their perception was accurately conveyed to colorblind readers [118].

References

[1] T. Helsten, M. Schwaederle, R. Kurzrock, Fibroblast growth factor receptor signaling in hereditary and neoplastic disease: biologic and clinical implications, Cancer Metastasis Rev. 34 (2015) 479–496.
[2] R. Goetz, M. Mohammadi, Exploring mechanisms of FGF signalling through the lens of structural biology, Nat. Rev. Mol. Cell Biol. 14 (2013) 166–180.
[3] D.M. Ornitz, N. Itoh, The fibroblast growth factor signaling pathway, Wiley Interdiscip. Rev. Dev. Biol. 4 (2015) 215–266.
[4] M.A. Lemmon, J. Schlessinger, Cell signaling by receptor tyrosine kinases, Cell 141 (2010) 1117–1134.
[5] C.M. Furdui, E.D. Lew, J. Schlessinger, K.S. Anderson, Autophosphorylation of FGFR1 kinase is mediated by a sequential and precisely ordered reaction, Mol. Cell 21 (2006) 711–717.
[6] N. Turner, R. Grose, Fibroblast growth factor signalling: from development to cancer, Nat. Rev. Cancer 10 (2010) 116–129.
[7] G. Chen, Y. Liu, R. Goetz, L. Fu, S. Jayaraman, M.C. Hu, et al., α-Klotho is a non-enzymatic molecular scaffold for FGF23 hormone signalling, Nature 553 (2018) 461–466.
[8] G. Manning, D.B. Whyte, R. Martinez, T. Hunter, S. Sudarsanam, The protein kinase complement of the human genome, Science 298 (2002) 1912–1934.
[9] L.E. Locascio, D.J. Donoghue, KIDs rule: regulatory phosphorylation of RTKs, Trends Biochem. Sci. 38 (2013) 75–84.
[10] D.R. Knighton, J.H. Zheng, L.F. Ten Eyck, V.A. Ashford, N.H. Xuong, S.S. Taylor, et al., Crystal structure of the catalytic subunit of cyclic adenosine monophosphate-dependent protein kinase, Science 253 (1991) 407–414.
[11] D.R. Knighton, J.H. Zheng, L.F. Ten Eyck, N.H. Xuong, S.S. Taylor, J.M. Sowadski, Structure of a peptide inhibitor bound to the catalytic subunit of cyclic adenosine monophosphate-dependent protein kinase, Science 253 (1991) 414–420.
[12] R.S. Vijayan, P. He, V. Modi, K.C. Duong-Ly, H. Ma, J.R. Peterson, et al., Conformational analysis of the DFG-out kinase motif and biochemical profiling of structurally validated type II inhibitors, J. Med. Chem. 58 (2015) 466–479.
[13] A.J. Kooistra, A. Volkamer, Kinase-centric computational drug development, Annu. Rep. Med. Chem. 50 (2017) 197–236.
[14] K. Shah, Y. Liu, C. Deirmengian, K.M. Shokat, Engineering unnatural nucleotide specificity for Rous sarcoma virus tyrosine kinase to uniquely label its direct substrates, Proc. Natl. Acad. Sci. U. S. A. 94 (1997) 3565–3570.
[15] Y. Liu, K. Shah, F. Yang, L. Witucki, K.M. Shokat, A molecular gate which controls unnatural ATP analogue recognition by the tyrosine kinase v-Src, Bioorg. Med. Chem. 6 (1998) 1219–1226.
[16] F. Zuccotto, E. Ardini, E. Casale, M. Angiolini, Through the "gatekeeper door": exploiting the active kinase conformation, J. Med. Chem. 53 (2010) 2691–2694.
[17] J. Zhou, J.A. Adams, Participation of ADP dissociation in the rate-determining step in cAMP-dependent protein kinase, Biochemistry 36 (1997) 15733–15738.
[18] A.C. Bastidas, M.S. Deal, J.M. Steichen, Y. Guo, J. Wu, S.S. Taylor, Phosphoryl transfer by protein kinase A is captured in a crystal lattice, J. Am. Chem. Soc. 135 (2013) 4788–4798.
[19] M.J. Knape, M. Ballez, N.C. Burghardt, B. Zimmermann, D. Bertinetti, A.P. Kornev, et al., Divalent metal ions control activity and inhibition of protein kinases, Metallomics 9 (2017) 1576–1584.
[20] H. Chen, J. Ma, W. Li, A.V. Eliseenkova, C. Xu, T.A. Neubert, et al., A molecular brake in the kinase hinge region regulates the activity of receptor tyrosine kinases, Mol. Cell 27 (2007) 717–730.
[21] A.P. Kornev, N.M. Haste, S.S. Taylor, L.F. Ten Eyck, Surface comparison of active and inactive protein kinases identifies a conserved activation mechanism, Proc. Natl. Acad. Sci. U. S. A. 103 (2006) 17783–17788.
[22] A.P. Kornev, S.S. Taylor, L.F. Ten Eyck, A helix scaffold for the assembly of active protein kinases, Proc. Natl. Acad. Sci. U. S. A. 105 (2008) 14377–14382.
[23] R. Roskoski Jr., MEK1/2 dual-specificity protein kinases: structure and regulation, Biochem. Biophys. Res. Commun. 417 (2012) 5–10.
[24] R. Roskoski Jr., Allosteric MEK1/2 inhibitors including cobimetanib and trametinib in the treatment of cutaneous melanomas, Pharmacol. Res. 117 (2017) 20–31.
[25] R. Roskoski Jr., ERK1/2 MAP kinases: structure, function, and regulation, Pharmacol. Res. 66 (2012) 105–143.
[26] R. Roskoski Jr., Targeting ERK1/2 protein-serine/threonine kinases in human cancers, Pharmacol. Res. 142 (2019) 151–168.
[27] R. Roskoski Jr., Anaplastic lymphoma kinase (ALK): structure, oncogenic activation, and pharmacological inhibition, Pharmacol. Res. 68 (2013) 68–94.
[28] R. Roskoski Jr., Anaplastic lymphoma kinase (ALK) inhibitors in the treatment of ALK-driven lung cancers, Pharmacol. Res. 117 (2017) 343–356.
[29] R. Roskoski Jr., ErbB/HER protein-tyrosine kinases: structures and small molecule inhibitors, Pharmacol. Res. 79 (2014) 34–74.
[30] R. Roskoski Jr., Small molecule inhibitors targeting the EGFR/ErbB family of protein-tyrosine kinases in human cancers, Pharmacol. Res. 139 (2019) 395–411.
[31] R. Roskoski Jr., Cyclin-dependent protein kinase inhibitors including palbociclib as anticancer drugs, Pharmacol. Res. 111 (2016) 784–803.
[32] R. Roskoski Jr., Cyclin-dependent protein serine/threonine kinase inhibitors as anticancer drugs, Pharmacol. Res. 139 (2019) 471–488.
[33] R. Roskoski Jr., Janus kinase (JAK) inhibitors in the treatment of inflammatory

and neoplastic diseases, Pharmacol. Res. 111 (2016) 784–803.
[34] R. Roskoski Jr., The role of small molecule Kit protein-tyrosine kinase inhibitors in the treatment of neoplastic disorders, Pharmacol. Res. 133 (2018) 35–52.
[35] R. Roskoski Jr., Targeting oncogenic Raf protein-serine/threonine kinases in human cancers, Pharmacol. Res. 135 (2018) 239–258.
[36] R. Roskoski Jr, A. Sadeghi-Nejad, Role of RET protein-tyrosine kinase inhibitors in the treatment RET-driven thyroid and lung cancers, Pharmacol. Res. 128 (2018) 1–17.
[37] R. Roskoski Jr., ROS1 protein-tyrosine kinase inhibitors in the treatment of ROS1 fusion protein-driven non-small cell lung cancers, Pharmacol. Res. 121 (2017) 202–212.
[38] R. Roskoski Jr., Ibrutinib inhibition of Bruton protein-tyrosine kinase (BTK) in the treatment of B cell neoplasms, Pharmacol. Res. 113 (2016) 395–408.
[39] R. Roskoski Jr., Vascular endothelial growth factor (VEGF) and VEGF receptor inhibitors in the treatment of renal cell carcinomas, Pharmacol. Res. 120 (2017) 116–132.
[40] R. Roskoski Jr., Src protein-tyrosine kinase structure, mechanism, and small molecule inhibitors, Pharmacol. Res. 94 (2015) 9–25.
[41] H.S. Meharena, P. Chang, M.M. Keshwani, K. Oruganty, A.K. Nene, N. Kannan, et al., Deciphering the structural basis of eukaryotic protein kinase regulation, PLoS Biol. 11 (2013) e1001690.
[42] O.P. van Linden, A.J. Kooistra, R. Leurs, I.J. de Esch, C. de Graaf, KLIFS: a knowledge-based structural database to navigate kinase-ligand interaction space, J. Med. Chem. 57 (2014) 249–277.
[43] R. Roskoski Jr., Properties of FDA-approved small molecule protein kinase inhibitors, Pharmacol. Res. 144 (2019) 19–50.
[44] K.D. Miller, L. Nogueira, A.B. Mariotto, J.H. Rowland, K.R. Yabroff, C.M. Alfano, et al., Cancer treatment and survivorship statistics, 2019, CA Cancer J. Clin. 69 (2019) 363–385.
[45] O. Sanli, J. Dobruch, M.A. Knowles, M. Burger, M. Alemozaffar, M.E. Nielsen, et al., Bladder cancer, Nat. Rev. Dis. Primers 3 (2017) 17022.
[46] P. Ghatalia, M. Zibelman, D.M. Geynisman, E. Plimack, Approved checkpoint inhibitors in bladder cancer: which drug should be used when? Ther. Adv. Med. Oncol. 10 (2018) 1758835918788310.
[47] K.S. Hanna, Erdafitinib to treat urothelial carcinoma, Drugs Today (Barc.) 55 (2019) 495–501.
[48] T. Helsten, S. Elkin, E. Arthur, B.N. Tomson, J. Carter, R. Kurzrock, The FGFR landscape in cancer: analysis of 4,853 tumors by next-generation sequencing, Clin. Cancer Res. 22 (2016) 259–267.
[49] Y.K. Chae, K. Ranganath, P.S. Hammerman, C. Vaklavas, N. Mohindra, A. Kalyan, et al., Inhibition of the fibroblast growth factor receptor (FGFR) pathway: the current landscape and barriers to clinical application, Oncotarget 8 (2017) 16052–16074.
[50] Y. Tanner, R.P. Grose, Dysregulated FGF signalling in neoplastic disorders, Semin. Cell Dev. Biol. 53 (2016) 126–135.
[51] H. Patani, T.D. Bunney, N. Thiyagarajan, R.A. Norman, D. Ogg, J. Breed, et al., Landscape of activating cancer mutations in FGFR kinases and their differential responses to inhibitors in clinical use, Oncotarget 7 (2016) 24252–24268.
[52] N. Stransky, E. Cerami, S. Schalm, J.L. Kim, C. Lengauer, The landscape of kinase fusions in cancer, Nat. Commun. 5 (2014) 4846.
[53] M. Katoh, Fibroblast growth factor receptors as treatment targets in clinical oncology, Nat. Rev. Clin. Oncol. 16 (2019) 105–122.
[54] J.J. Keats, T. Reiman, A.R. Belch, L.M. Pilarski, Ten years and counting: so what do we know about t(4;14)(p16;q32) multiple myeloma, Leuk. Lymphoma 47 (2006) 2289–2300.
[55] J. Wesche, K. Haglund, E.M. Haugsten, Fibroblast growth factors and their receptors in cancer, Biochem. J. 437 (2011) 199–213.
[56] A.C. Dar, K.M. Shokat, The evolution of protein kinase inhibitors from antagonists to agonists of cellular signaling, Annu. Rev. Biochem. 80 (2011) 769–795.
[57] L.K. Gavrin, E. Saiah, Approaches to discover non-ATP site inhibitors, Med. Chem. Res. 4 (2013) 41.
[58] V. Lamba, I. Ghosh, New directions in targeting protein kinases: focusing upon true allosteric and bivalent inhibitors, Curr. Pharm. Des. 18 (2012) 2936–2945.
[59] T.K. Johnson, M.B. Soellner, Bivalent inhibitors of c-Src tyrosine kinase that bind a regulatory domain, Bioconjug. Chem. 27 (2016) 1745–1749.
[60] R.Jr. Roskoski, Classification of small molecule protein kinase inhibitors based upon the structures of their drug-enzyme complexes, Pharmacol. Res. 103 (2016) 26–48.
[61] R.A. Copeland, The drug-target residence time model: a 10-year retrospective, Nat. Rev. Drug Discov. 15 (2016) 87–95.
[62] J.J. Liao, Molecular recognition of protein kinase binding pockets for design of potent and selective kinase inhibitors, J. Med. Chem. 50 (2007) 409–424.
[63] F. Carles, S. Bourg, C. Meyer, P. Bonnet, PKIDB: a curated, annotated and updated database of protein kinase inhibitors in clinical trials, Molecules 23 (2018), https://doi.org/10.3390/molecules23040908 pii: E908.
[64] C.A. Lipinski, F. Lombardo, B.W. Dominy, P.J. Feeney, Experimental and computational approaches to estimate solubility and permeability in drug discovery and development settings, Adv. Drug Deliv. Rev. 46 (2001) 3–26.
[65] T.P.S. Perera, E. Jovcheva, L. Mevellec, J. Vialard, D. De Lange, T. Verhulst, et al., Discovery and pharmacological characterization of JNJ-42756493 (erdafitinib), a functionally selective small-molecule FGFR family inhibitor, Mol. Cancer Ther. 16 (2017) 1010–1020.
[66] Y. Loriot, A. Necchi, S.H. Park, J. Garcia-Donas, R. Huddart, E. Burgess, et al., Erdafitinib in locally advanced or metastatic urothelial carcinoma, N. Engl. J. Med. 381 (2019) 338–348.
[67] R. Dienstmann, J. Rodon, A. Prat, J. Perez-Garcia, B. Adamo, E. Felip, et al., Genomic aberrations in the FGFR pathway: opportunities for targeted therapies in solid tumors, Ann. Oncol. 25 (2014) 552–563.
[68] J. Gattineni, P. Alphonse, Q. Zhang, N. Mathews, C.M. Bates, M. Baum, Regulation of renal phosphate transport by FGF23 is mediated by FGFR1 and FGFR4, Am. J. Physiol. Renal Physiol. 306 (2014) F351–F358.
[69] R.D. Kim, D. Sarker, T. Meyer, T. Yau, T. Macarulla, J.W. Park, et al., First-in-human phase I study of fisogatinib (BLU-554) validates aberrant fibroblast growth factor 19 signaling as a driver event in hepatocellular carcinoma, Cancer Discov. (2019) pii: CD-19-0555.
[70] X. Han, J. Yang, L. Li, J. Huang, G. King, L.D. Quarles, Conditional deletion of Fgfr1 in the proximal and distal tubule identifies distinct roles in phosphate and calcium transport, PLoS One 11 (2) (2016) e0147845.
[71] F. Facchinetti, A. Hollebecque, R. Bahleda, Y. Loriot, K.A. Olaussen, C. Massard, et al., Facts and new hopes on selective FGFR inhibitors in solid tumors, Clin. Cancer Res. (2019), https://doi.org/10.1158/1078-0432.CCR-19-2035 pii: clincanres.2035.2019.
[72] W.S. Huang, C.A. Metcalf, R. Sundaramoorthi, Y. Wang, D. Zou, R.M. Thomas, et al., Discovery of 3-[2-(imidazo[1,2-*b*]pyridazin-3-yl)ethynyl]-4-methyl-N-{4-[(4-methylpiperazin-1-yl)methyl]-3-(trifluoromethyl)phenyl}benzamide (AP24534), a potent, orally active pan-inhibitor of Breakpoint Cluster Region-Abelson (BCR-ABL) kinase including the T315I gatekeeper mutant, J. Med. Chem. 53 (2010) 4701–4719.
[73] M.C. Müller, F. Cervantes, H. Hjorth-Hansen, J.J.W.M. Janssen, D. Milojkovic, D. Rea, et al., Ponatinib in chronic myeloid leukemia (CML): consensus on patient treatment and management from a European expert panel, Crit. Rev. Oncol. Hematol. 120 (2017) 52–59.
[74] E. Jabbour, H. Kantarjian, Chronic myeloid leukemia: 2018 update on diagnosis, therapy and monitoring, Am. J. Hematol. 93 (2018) 442–459.
[75] M. Katoh, FGFR inhibitors: effects on cancer cells, tumor microenvironment and whole-body homeostasis (Review), Int. J. Mol. Med. 38 (1) (2016) 3–15.
[76] J.A. Tucker, T. Klein, J. Breed, A.L. Breeze, R. Overman, C. Phillips, et al., Structural insights into FGFR kinase isoform selectivity: diverse binding modes of AZD4547 and ponatinib in complex with FGFR1 and FGFR4, Structure 22 (2014) 1764–1774.
[77] E. Lesca, A. Lammens, R. Huber, M. Augustin, Structural analysis of the human fibroblast growth factor receptor 4 kinase, J. Mol. Biol. 426 (2014) 3744–3756.
[78] Z. Huang, L. Tan, H. Wang, Y. Liu, S. Blais, J. Deng, et al., DFG-out mode of inhibition by an irreversible type-1 inhibitor capable of overcoming gate-keeper mutations in FGF receptors, ACS Chem. Biol. 10 (2015) 299–309.
[79] T.D. Bunney, S. Wan, N. Thiyagarajan, L. Sutto, S.V. Williams, P. Ashford, et al., The effect of mutations on drug sensitivity and kinase activity of fibroblast growth factor receptors: a combined experimental and theoretical study, EBioMedicine 2 (2015) 194–204.
[80] T. Klein, N. Vajpai, J.J. Phillips, G. Davies, G.A. Holdgate, C. Phillips, et al., Structural and dynamic insights into the energetics of activation loop rearrangement in FGFR1 kinase, Nat. Commun. 6 (2015) 7877.
[81] C.D. Sohl, M.R. Ryan, B. Luo, K.M. Frey, K.S. Anderson, Illuminating the molecular mechanisms of tyrosine kinase inhibitor resistance for the FGFR1 gatekeeper mutation: the Achilles' heel of targeted therapy, ACS Chem. Biol. 10 (2015) 1319–1329.
[82] E. Van Cutsem, Y.J. Bang, W. Mansoor, R.D. Petty, Y. Chao, D. Cunningham, et al., A randomized, open-label study of the efficacy and safety of AZD4547 monotherapy versus paclitaxel for the treatment of advanced gastric adenocarcinoma with FGFR2 polysomy or gene amplification, Ann. Oncol. 28 (2017) 1316–1324.
[83] Y. Nakanishi, N. Akiyama, T. Tsukaguchi, T. Fujii, K. Sakata, H. Sase, et al., The fibroblast growth factor receptor genetic status as a potential predictor of the sensitivity to CH5183284/Debio 1347, a novel selective FGFR inhibitor, Mol. Cancer Ther. 13 (2014) 2547–2558.
[84] H. Ebiike, N. Taka, M. Matsushita, M. Ohmori, K. Takami, I. Hyohdoh, et al., Discovery of [5-amino-1-(2-methyl-3H-benzimidazol-5-yl)pyrazol-4-yl]-(1H-indol-2-yl)methanone (CH5183284/Debio 1347), an orally available and selective fibroblast growth factor receptor (FGFR) inhibitor, J. Med. Chem. 59 (2016) 10586–10600.
[85] V. Guagnano, P. Furet, C. Spanka, V. Bordas, M. Le Douget, C. Stamm, et al., Discovery of 3-(2,6-dichloro-3,5-dimethoxy-phenyl)-1-{6-[4-(4-ethyl-piperazin-1-yl)-phenylamino]-pyrimidin-4-yl}-1-methyl-urea (NVP-BGJ398), a potent and selective inhibitor of the fibroblast growth factor receptor family of receptor tyrosine kinase, J. Med. Chem. 54 (2011) 7066–7083.
[86] L. Nogova, L.V. Sequist, J.M. Perez Garcia, F. Andre, J.P. Delord, M. Hidalgo, et al., Evaluation of BGJ398, a fibroblast growth factor receptor 1-3 kinase inhibitor, in patients with advanced solid tumors harboring genetic alterations in fibroblast growth factor receptors: results of a global phase I, dose-escalation and dose-expansion study, J. Clin. Oncol. 35 (2017) 157–165.
[87] S. Zschäbitz, C. Grüllich, Lenvantinib: a tyrosine kinase inhibitor of VEGFR 1-3, FGFR 1-4, PDGFRα, KIT and RET, Recent Results Cancer Res. 211 (2018) 187–198.
[88] Y. Yamamoto, J. Matsui, T. Matsushima, H. Obaishi, K. Miyazaki, K. Nakamura, et al., Lenvatinib, an angiogenesis inhibitor targeting VEGFR/FGFR, shows broad antitumor activity in human tumor xenograft models associated with microvessel density and pericyte coverage, Vasc. Cell 6 (2014) 18.
[89] M. Matsuki, T. Hoshi, Y. Yamamoto, M. Ikemori-Kawada, Y. Minoshima, Y. Funahashi, et al., Lenvatinib inhibits angiogenesis and tumor fibroblast growth factor signaling pathways in human hepatocellular carcinoma models, Cancer Med. 7 (2018) 2641–2653.
[90] G. Zhao, W.Y. Li, D. Chen, J.R. Henry, H.Y. Li, Z. Chen, et al., A novel, selective inhibitor of fibroblast growth factor receptors that shows a potent broad spectrum of antitumor activity in several tumor xenograft models, Mol. Cancer Ther. 10

(2011) 2200–2210.
[91] D. Wu, M. Guo, M.A. Philips, L. Qu, L. Jiang, J. Li, et al., Crystal structure of the FGFR4/LY2874455 complex reveals insights into the pan-FGFR selectivity of LY2874455, PLoS One 11 (2016) e0162491.
[92] M. Michael, Y.J. Bang, Y.S. Park, Y.K. Kang, T.M. Kim, O. Hamid, et al., A phase 1 study of LY2874455, an oral selective pan-FGFR inhibitor, in patients with advanced cancer, Target. Oncol. 12 (2017) 463–474.
[93] Y. Zhou, Y. Chen, L. Tong, H. Xie, W. Wen, J. Zhang, et al., AL3810, a multi-tyrosine kinase inhibitor, exhibits potent anti-angiogenic and anti-tumour activity via targeting VEGFR, FGFR and PDGFR, J. Cell. Mol. Med. 16 (2012) 2321–2330.
[94] M. Kalyukina, Y. Yosaatmadja, M.J. Middleditch, A.V. Patterson, J.B. Smaill, C.J. Squire, TAS-120 cancer target binding: defining reactivity and revealing the first fibroblast growth factor receptor 1 (FGFR1) irreversible structure, ChemMedChem 14 (2019) 494–500.
[95] L. Goyal, L. Shi, L.Y. Liu, F. Fece de la Cruz, J.K. Lennerz, S. Raghavan, et al., TAS-120 overcomes resistance to ATP-competitive FGFR inhibitors in patients with FGFR2 fusion-positive intrahepatic cholangiocarcinoma, Cancer Discov. 9 (2019) 1064–1079.
[96] A. Weiss, F. Adler, A. Buhles, C. Stamm, R.A. Fairhurst, M. Kiffe, et al., FGF401, a first-in-class highly selective and potent FGFR4 inhibitor for the treatment of FGF19-driven hepatocellular cancer, Mol. Cancer Ther. (2019), https://doi.org/10.1158/1535-7163.MCT-18-1291 pii: molcanther.1291.2018.
[97] Z. Zhou, X. Chen, Y. Fu, Y. Zhang, S. Dai, J. Li, et al., Characterization of FGF401 as a reversible covalent inhibitor of fibroblast growth factor receptor 4, Chem. Commun. (Camb.) 55 (2019) 5890–5893.
[98] J.J. Joshi, H. Coffey, E. Corcoran, J. Tsai, C.L. Huang, K. Ichikawa, et al., H3B-6527 is a potent and selective inhibitor of FGFR4 in FGF19-driven hepatocellular carcinoma, Cancer Res. 77 (2017) 6999–7013.
[99] G.J. Roth, A. Heckel, F. Colbatzky, S. Handschuh, J. Kley, T. Lehmann-Lintz, et al., Design, synthesis, and evaluation of indolinones as triple angiokinase inhibitors and the discovery of a highly specific 6-methoxycarbonyl-substituted indolinone (BIBF 1120), J. Med. Chem. 52 (2009) 4466–4480.
[100] S.S. Terzyan, T. Shen, X. Liu, Q. Huang, P. Teng, M. Zhou, et al., Structural basis of resistance of mutant RET protein-tyrosine kinase to its inhibitors nintedanib and vandetanib, J. Biol. Chem. 294 (2019) 10428–10437.
[101] P.A. Harris, A. Boloor, M. Cheung, R. Kumar, R.M. Crosby, R.G. Davis-Ward, et al., Discovery of 5-[[4-[(2,3-dimethyl-2H-indazol-6-yl)methylamino]-2-pyrimidinyl] amino]-2-methyl-benzenesulfonamide (pazopanib), a novel and potent vascular endothelial growth factor receptor inhibitor, J. Med. Chem. 51 (2008) 4632–4640.
[102] C. Chauvin, A. Leruste, A. Tauziede-Espariat, M. Andrianteranagna, D. Surdez, A. Lescure, et al., High-throughput drug screening identifies pazopanib and clofilium tosylate as promising treatments for malignant rhabdoid tumors, Cell Rep. 21 (2017) 1737–1745.
[103] S. Dai, Z. Zhou, Z. Chen, G. Xu, Y. Chen, Fibroblast growth factor receptors (FGFRs): structures and small molecule inhibitors, Cells 8 (2019) pii: E614.
[104] M.P. Collin, M. Lobell, W. Hübsch, D. Brohm, H. Schirok, R. Jautelat, et al., Discovery of rogaratinib (BAY 1163877): a pan-FGFR inhibitor, ChemMedChem 13 (2018) 437–445.
[105] M. Schuler, B.C. Cho, C.M. Sayehli, A. Navarro, R.A. Soo, H. Richly, et al., Rogaratinib in patients with advanced cancers selected by FGFR mRNA expression: a phase 1 dose-escalation and dose-expansion study, Lancet Oncol. 20 (2019) 1454–1466.
[106] M.A. Hatlen, O. Schmidt-Kittler, C.A. Sherwin, E. Rozsahegyi, N. Rubin, M.P. Sheets, et al., Acquired on-target clinical resistance validates FGFR4 as a driver of hepatocellular carcinoma, Cancer Discov. (2019) pii: CD-19-0367.
[107] K.A. Brameld, T.D. Owens, E. Verner, E. Venetsanakos, J.M. Bradshaw, V.T. Phan, et al., Discovery of the irreversible covalent FGFR inhibitor 8-(3-(4-acryloylpiperazin-1-yl)propyl)-6-(2,6-dichloro-3,5-dimethoxyphenyl)-2-(methylamino) pyrido[2,3-*d*]pyrimidin-7(8H)-one (PRN1371) for the treatment of solid tumors, J. Med. Chem. 60 (2017) 6516–6527.
[108] R. Roskoski Jr., The role of small molecule platelet-derived growth factor receptor (PDGFR) inhibitors in the treatment of neoplastic disorders, Pharmacol. Res. 129 (2018) 65–83.
[109] M.B. Laederich, W.A. Horton, Achondroplasia: pathogenesis and implications for future treatment, Curr. Opin. Pediatr. 22 (2010) 516–523.
[110] P.L. Tavormina, R. Shiang, L.M. Thompson, Y.Z. Zhu, D.J. Wilkin, R.S. Lachman, et al., Thanatophoric dysplasia (types I and II) caused by distinct mutations in fibroblast growth factor receptor 3, Nat. Genet. 9 (1995) 321–328.
[111] R. Rai, J. Iwanaga, G. Dupont, R.J. Oskouian, M. Loukas, W.J. Oakes, et al., Pfeiffer type 2 syndrome: review with updates on its genetics and molecular biology, Childs Nerv. Syst. (2019), https://doi.org/10.1007/s00381-019-04082-7.
[112] R. Roskoski Jr., A historical overview of protein kinases and their targeted small molecule inhibitors, Pharmacol. Res. 100 (2015) 1–23.
[113] L. Goyal, S.K. Saha, L.Y. Liu, G. Siravegna, I. Leshchiner, L.G. Ahronian, et al., Polyclonal secondary *FGFR2* mutations drive acquired resistance to FGFR inhibition in patients with FGFR2 fusion-positive cholangiocarcinoma, Cancer Discov. 7 (2017) 252–263.
[114] G.K. Kanev, C. de Graaf, I.J.P. de Esch, R. Leurs, T. Würdinger, B.A. Westerman, et al., The landscape of atypical and eukaryotic protein kinases, Trends Pharmacol. Sci. (2019) pii: S0165-6147(19)30213–5.
[115] R. Nadal, J. Bellmunt, Management of metastatic bladder cancer, Cancer Treat. Rev. 76 (2019) 10–21.
[116] L. Amable, Cisplatin resistance and opportunities for precision medicine, Pharmacol. Res. 106 (2016) 27–36.
[117] A. Giacomini, P. Chiodelli, S. Matarazzo, M. Rusnati, M. Presta, R. Ronca, Blocking the FGF/FGFR system as a "two-compartment" antiangiogenic/antitumor approach in cancer therapy, Pharmacol. Res. 107 (2016) 172–185.
[118] R.Jr. Roskoski, Guidelines for preparing color figures for everyone including the colorblind, Pharmacol. Res. 119 (2017) 240–241 Erratum in: Pharmacol Res 2019;139:569.